



## Can compliant fault zones be used to measure absolute stresses in the upper crust?

E. H. Hearn<sup>1</sup> and Y. Fialko<sup>2</sup>

Received 27 June 2008; revised 16 November 2008; accepted 22 January 2009; published 10 April 2009.

[1] Geodetic and seismic observations reveal long-lived zones with reduced elastic moduli along active crustal faults. These fault zones localize strain from nearby earthquakes, consistent with the response of a compliant, elastic layer. Fault zone trapped wave studies documented a small reduction in P and S wave velocities along the Johnson Valley Fault caused by the 1999 Hector Mine earthquake. This reduction presumably perturbed a permanent compliant structure associated with the fault. The inferred changes in the fault zone compliance may produce a measurable deformation in response to background (tectonic) stresses. This deformation should have the same sense as the background stress, rather than the coseismic stress change. Here we investigate how the observed deformation of compliant zones in the Mojave Desert can be used to constrain the fault zone structure and stresses in the upper crust. We find that gravitational contraction of the coseismically softened zones should cause centimeters of coseismic subsidence of both the compliant zones and the surrounding region, unless the compliant fault zones are shallow and narrow, or essentially incompressible. We prefer the latter interpretation because profiles of line of sight displacements across compliant zones cannot be fit by a narrow, shallow compliant zone. Strain of the Camp Rock and Pinto Mountain fault zones during the Hector Mine and Landers earthquakes suggests that background deviatoric stresses are broadly consistent with Mohr-Coulomb theory in the Mojave upper crust (with  $\mu \geq 0.7$ ). Large uncertainties in Mojave compliant zone properties and geometry preclude more precise estimates of crustal stresses in this region. With improved imaging of the geometry and elastic properties of compliant zones, and with precise measurements of their strain in response to future earthquakes, the modeling approach we describe here may eventually provide robust estimates of absolute crustal stress.

**Citation:** Hearn, E. H., and Y. Fialko (2009), Can compliant fault zones be used to measure absolute stresses in the upper crust?, *J. Geophys. Res.*, *114*, B04403, doi:10.1029/2008JB005901.

### 1. Introduction

[2] Active crustal faults are often associated with long-lived zones of reduced rigidity compared to the host rock (e.g., summary by Lewis *et al.* [2005], Li *et al.* [1990], and Fialko *et al.* [2002]). Given a sudden stress change (e.g., from a nearby earthquake), these fault zones concentrate strain, resulting in small-wavelength “wrinkles” of positive or negative range change along active faults as documented by interferometric synthetic aperture radar (InSAR) observations (Figure 1). Interpretations of geodetic data suggest that these zones may be 1 to 2 km wide and are characterized by a significant (factor of 2 to 3) reduction in the shear modulus  $G$  relative to the surrounding rock [Fialko *et al.*,

2002; Fialko, 2004; Hamiel and Fialko, 2007]. Seismic studies suggest a similar contrast in  $G$ ; most of the imaged zones appear to be about 100 to 300 m wide [e.g., Li *et al.*, 1990; Lewis *et al.*, 2005; Peng *et al.*, 2003], although the fault zone widths up to 1–2 km have been documented as well [Spudich and Olsen, 2001; Cochran *et al.*, 2009]. Some of the difference in estimated compliant zone widths might arise from the frequency dependence of the elastic moduli of rocks. Geodetic observations sample static (vanishing frequency) elastic properties and seismic observations sample dynamic (high-frequency) elastic properties. Various compilations show that the static rigidity is consistently lower than the dynamic rigidity [e.g., Eissa and Kazi, 1988; Ciccotti and Mulargia, 2004; Ide, 1936], particularly for rocks near the Earth’s surface. However, it is not clear whether the rigidity contrast between the fault zone material and the host rocks is also frequency-dependent.

[3] Estimates of the depths of compliant fault zones also vary, from a few kilometers [e.g., Peng *et al.*, 2003] to the entire thickness of the seismogenic zone [Li *et al.*, 1990; Fialko *et al.*, 2002]. Fault evolution models suggest that the

<sup>1</sup>Department of Earth and Ocean Sciences, University of British Columbia, Vancouver, British Columbia, Canada.

<sup>2</sup>Institute of Geophysics and Planetary Physics, Scripps Institution of Oceanography, University of California, San Diego, La Jolla, California, USA.

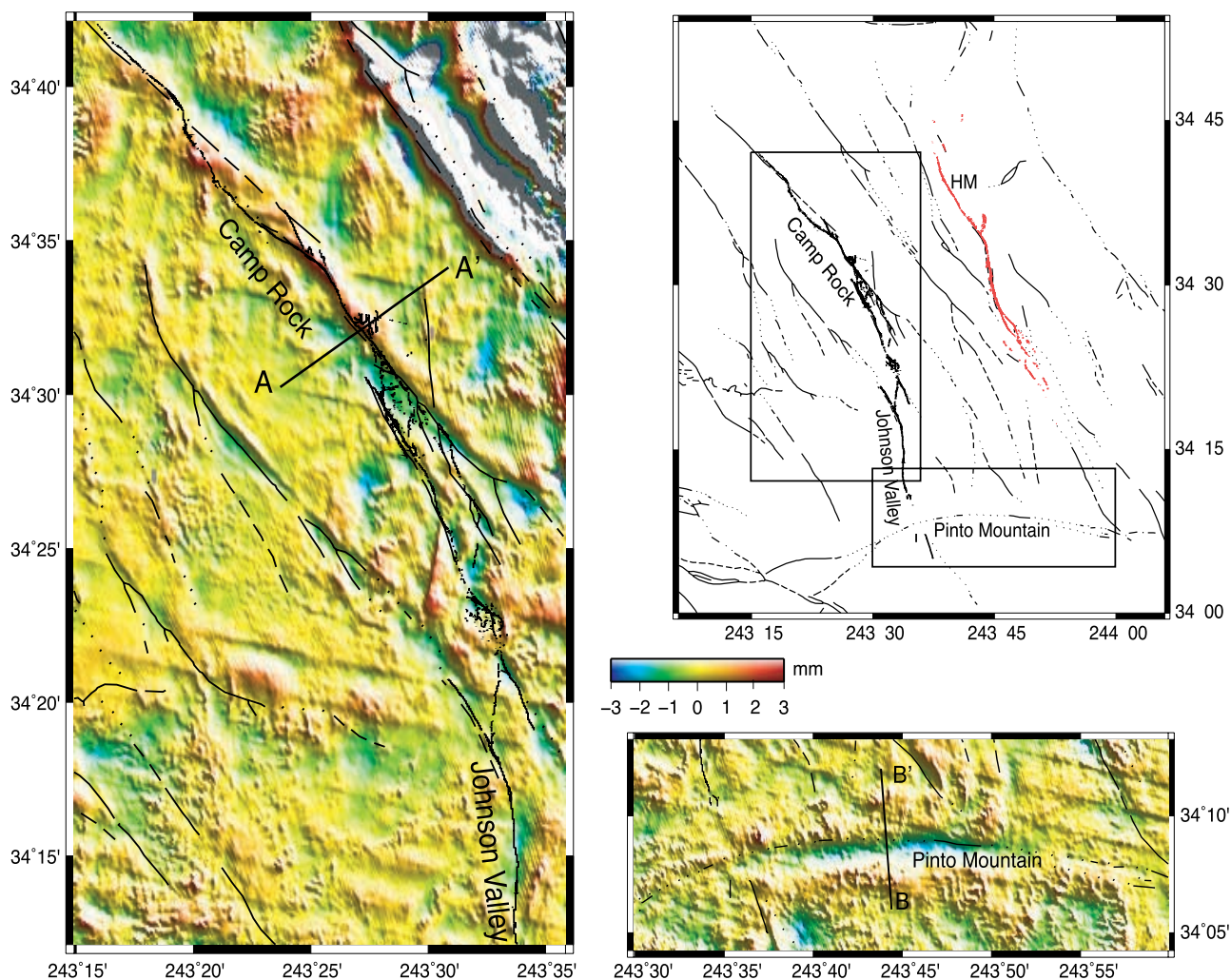


**Figure 1.** Map of the epicentral area of the Hector Mine earthquake (HM, red curvy line) showing known Quaternary faults. Color plots denote high-pass-filtered line-of-sight displacements caused by the Hector Mine earthquake on the (left) Landers and (bottom) Pinto Mountain faults. Coseismic interferogram was constructed from acquisitions of the ERS-2 satellite, track 127, taken on 13 January and 20 October 1999 [Fialko *et al.*, 2002].

depth of a permanent compliant zone along a strike-slip fault in a crust with damage-controlled brittle rheology is less than about 7 km [Finzi *et al.*, 2009].

[4] Coseismic damage and softening of fault zones ruptured by earthquakes have been reported in a number of studies [e.g., Peng and Ben Zion, 2006; Li *et al.*, 2006; Brenguier *et al.*, 2008]. Studies of fault zone trapped waves have revealed postseismic healing in earthquake rupture zones and along nearby faults following the 1992 Landers earthquake [e.g., Li and Vidale, 2001; Li *et al.*, 2003]. The Hector Mine earthquake disrupted this postseismic healing along the Johnson Valley Fault, about 30 km west from the epicenter of the 1999 Hector Mine earthquake [Vidale and Li, 2003]. A coseismic decrease in both  $V_p$  and  $V_s$  in the Johnson Valley fault zone was observed, to a depth of approximately 5 km (though the depth extent of the coseismic velocity perturbation is rather poorly constrained). This decrease in the fault zone rigidity should have caused a component of deformation consistent with the sense of background tectonic stress (Figure 2).

[5] The sense of coseismic strain of several fault zones in the neighborhood of the Hector Mine rupture, including the Calico, Rodman, and Pinto Mountain faults, was found to be compatible with coseismic stress changes, and opposite to the sense one would expect from the regional stress field [Fialko *et al.*, 2002; Fialko, 2004]. These observations suggest either low deviatoric stresses in the upper crust, or negligible coseismic softening of the preexisting compliant fault zones. Unfortunately, no seismic data are available to discriminate between the two possibilities.

[6] Here, we investigate the effect of coseismic changes in both the stress field and the rigidity of compliant fault zones in the Mojave desert. Since crustal stress and compliant zone geometry are not well constrained, we investigate a range of plausible parameters. In section 2, we present theoretical analysis of the fault zone response to coseismic loading assuming homogeneous stresses. Readers interested in numerical results from the Eastern California Shear Zone should skip to section 3, where we place constraints on the fault zone properties and geometry, as

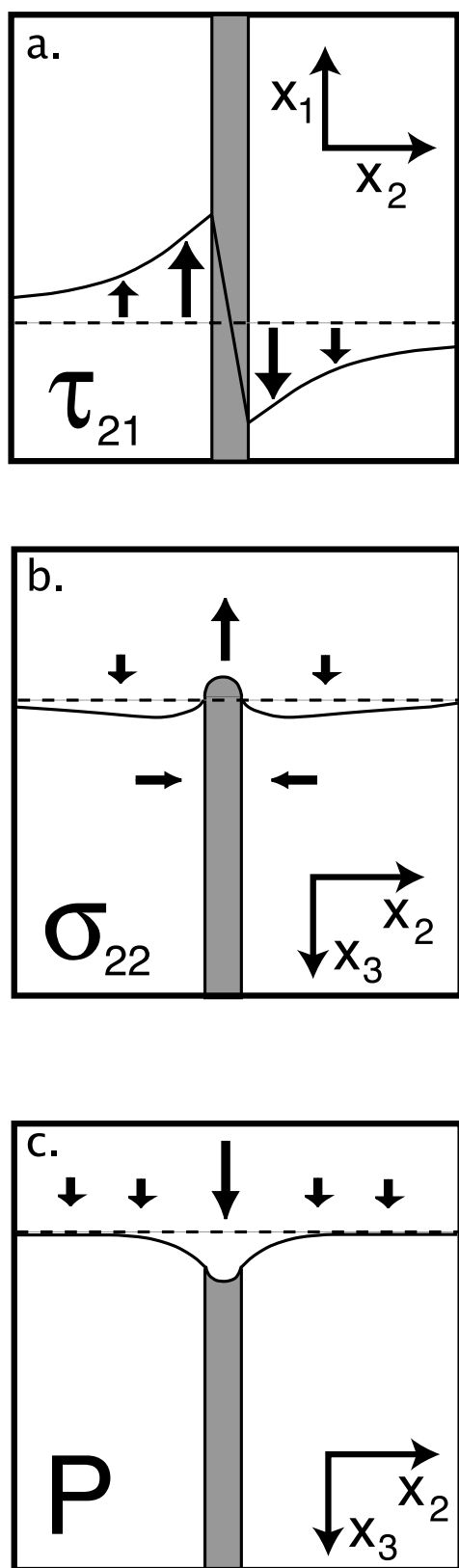


**Figure 2.** Deformation of a coseismically softened compliant zone. Arrows schematically represent displacements due to background stresses acting on a compliant zone, which softens coseismically. Deformation contributions from (a) shear stress, (b) compressive normal stress, and (c) lithostatic pressure are shown.

well as the regional stress field, by comparing the model predictions to InSAR observations.

## 2. Compliant Zones as Stress Meters: Theory

[7] The enhanced coseismic strain  $\delta\varepsilon$  in a compliant fault zone is the difference between the compliant zone strain, and strain in the surrounding crust, due to a nearby earthquake.  $\delta\varepsilon$  may result from the coseismic stress changes  $\delta\sigma$  acting on a heterogeneous elastic structure, and from possible coseismic damage and softening of the fault zone in the presence of absolute (tectonic) stress  $\sigma_0$ ,

$$\delta\varepsilon \sim \frac{G - G'}{GG'} \delta\sigma - \frac{\sigma_0}{G^2} \delta G', \quad (1)$$

where  $G'$  and  $G$  are the effective elastic moduli of the fault zone and host rocks, respectively, and  $\delta G'$  is the coseismic change in the fault zone modulus. We assume that the coseismic damage is limited to a compliant fault zone (CZ), and does not occur in the ambient rocks. Effects of coseismic stress changes on a preexisting compliant structure (first term on the right-hand side of equation (1)) are reasonably well understood [e.g., *Fialko et al.*, 2002]. The second term on the right-hand side of equation (1) is a first-order term in a Taylor series expansion of  $\sigma_0/G'$  about a small perturbation in  $G'$ . In this section, we investigate analytical solutions for CZ deformation due to coseismic softening.

[8] The geometry of this problem is outlined in Figure 3. A vertical strike-slip fault in an elastic half-space is embedded in a compliant zone having a constant width  $2w$  and extending from the surface of the half-space to depth  $h$ . We introduce a Cartesian coordinate system  $(x_1, x_2, x_3)$  such that the fault plane contains  $x_1$  and  $x_3$  axes, the origin is at the Earth's surface, axis  $x_3$  is vertical (positive downward), and axis  $x_2$  is horizontal and normal to the fault. The state of stress in the surrounding crust is characterized by three principal stresses  $(\sigma_1, \sigma_2, \sigma_3)$  such that the maximum and least compressive stresses ( $\sigma_1$  and  $\sigma_3$ , respectively) are horizontal, and the intermediate stress is lithostatic,  $\sigma_2 = -\rho_r g x_3$ , where  $\rho_r$  is the rock density, and  $g$  is the gravitational acceleration. The maximum compression axis makes

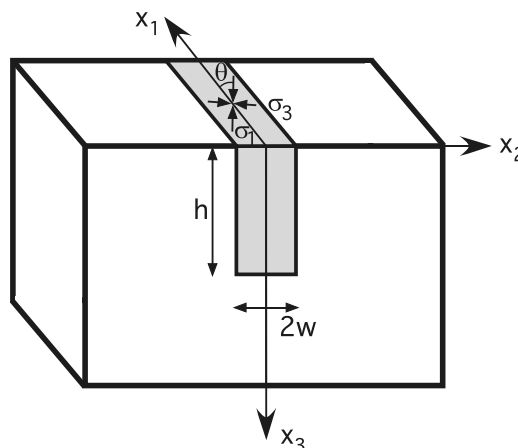


**Figure 3.** Schematic cartoon of a compliant zone, showing geometric parameters and coordinates.

an angle  $\theta$  with the fault trace. The principal stresses are allowed to increase with depth, but are presumed to have a constant orientation and magnitude along strike ( $x_1$  direction). Under these assumptions, deformation due to a fault zone can be represented by a superposition of two two-dimensional solutions: a plane strain solution involving fault-normal stress  $\sigma_n$ , and antiplane strain solution involving shear stress in the direction of fault slip  $\sigma_s$ . The corresponding stresses are readily expressed in terms of the principal stresses as follows [Malvern, 1969, Suppe, 1985]:

$$\sigma_n = \frac{1}{2}(\sigma_1 + \sigma_3) - \frac{1}{2}(\sigma_1 - \sigma_3) \cos 2\theta \quad (2)$$

$$\sigma_s = \frac{1}{2}(\sigma_1 - \sigma_3) \sin 2\theta. \quad (3)$$

Maximum stresses attainable on a fault are given by the Mohr-Coulomb failure criterion,

$$\sigma_s = \mu(\sigma_n - p) + c, \quad (4)$$

where  $\mu = 0.6$  is the coefficient of static friction,  $c$  is the cohesive stress (i.e., the fault strength at zero effective stress), and  $p$  is the pore fluid pressure. Hereafter, we assume that the pore pressure is hydrostatic,  $p = -\rho_w g x_3$ , where  $\rho_w$  is the density of water; and that  $c$  is negligible. Prior to the onset of fault slip given by condition (4), rock within the fault zone obeys the linear elasticity relationship given by Hooke's law,

$$\varepsilon_{ij} = \frac{1}{2(1+\nu)G'} [(1+\nu)\sigma_{ij} - \nu\delta_{ij}\sigma_{kk}], \quad (5)$$

where  $G'$  is the shear modulus,  $\nu$  is the Poisson ratio, and  $\delta_{ij}$  is the Kronecker's delta.

[9] First, we consider the case of an antiplane deformation. From equation (5), elastic shear strain within the fault zone is

$$\varepsilon_{12} = \frac{\sigma_{12}}{2G'}, \quad (6)$$

where  $\sigma_{12} = \sigma_s$  is shear stress resolved on a fault. A perturbation in the shear modulus  $\delta G'$  will result in a strain increment

$$\delta\varepsilon_{12} = -\frac{\sigma_{12}}{2G'} \frac{\delta G'}{G'}, \quad (7)$$

and the effective shear displacement across the fault zone  $\delta u_1 = 4\delta\varepsilon_{12}w$ . Assuming a constant  $\delta G'$ , the magnitude of shear initially increases with depth proportionally to the magnitude of shear stress  $\sigma_s$ , and then tapers to zero toward the bottom of the damage zone. Adopting  $\delta G'/G' = 1-2\%$  [Vidale and Li, 2003],  $w = 10^2-10^3$  m [Spudich and Olsen, 2001; Fialko et al., 2002; Hamiel and Fialko, 2007; Cochran et al., 2009],  $G' = 3-10$  GPa,  $\sigma_s = 10-50$  MPa as representative values, one infers  $\delta u_1$  of the order of a few millimeters to a few tens of centimeters. This may be

compared to displacements of a few centimeters resulting from the elastic response of compliant fault zones to the coseismic stress changes [e.g., Fialko et al., 2002; Fialko, 2004]. Depending on details of  $\sigma_s$  increase with depth, deeper shear due to the fault zone softening results in smaller amplitudes and larger wavelength of deformation at the surface, and may be difficult to detect, especially in the presence of coseismic deformation due to a nearby earthquake. Nonetheless, for high-end parameters considered above, deformation due to perturbations in the effective elastic moduli may be detected with precise geodetic measurements, and therefore provide insight into the magnitude of absolute shear stress at depth.

[10] Next, we consider the plane strain problem. Coseismic increases in the fault zone compliance result in two opposing effects: gravity causes the softened zone to subside, while the fault-normal stress gives rise to uplift due to a Poissonian expansion. It is of interest to evaluate these effects, as measurements of vertical displacements may provide an independent constraint on coseismic changes in the effective elastic moduli (i.e., in addition to seismic tomography). The condition of plane strain implies  $\varepsilon_{11} = 0$  and

$$\sigma_{11} = \nu(\sigma_{22} + \sigma_{33}). \quad (8)$$

Making use of relationship (8), from equation (5) one obtains the following expression for the vertical component of strain:

$$\varepsilon_{33} = \frac{1}{2G'} [(1-\nu)\sigma_{33} - \nu\sigma_{22}] = -\frac{\rho_w g x_3}{2G'} [1 - \nu(1+\lambda)], \quad (9)$$

where  $\lambda = -\sigma_n/\rho_w g x_3$  is the ratio of the fault-normal stress to the lithostatic pressure. Vertical deformation due to perturbations in the elastic moduli is

$$\delta\varepsilon_{33} = \frac{\partial\varepsilon_{33}}{\partial G'} \delta G' + \frac{\partial\varepsilon_{33}}{\partial\nu} \delta\nu = \frac{\rho_w g x_3}{2G'} \cdot \left[ (1-\nu(1+\lambda)) \frac{\partial G'}{G'} + \nu(1+\lambda) \frac{\partial\nu}{\nu} \right]. \quad (10)$$

The fault-normal stress depends on magnitudes of the maximum and least principal stresses  $\sigma_1$  and  $\sigma_3$ , and angle  $\theta$  between the fault plane and the maximum compression axis (equation (2)). The maximum differential stress beyond which optimally oriented faults begin to slip is constrained by a condition  $\sigma_1 < K(\sigma_3 - p) + p$ , where  $K = (\mu + \sqrt{1 + \mu^2})^2$  is the Earth pressure coefficient [Sibson, 1974; Suppe, 1985]. We estimate the lower bound on the fault-normal stress by assuming  $\theta = 30^\circ$  (close to optimal orientation) and  $\sigma_1 \rightarrow \sigma_2$  (corresponding to a transtensional regime). The upper bound on  $\sigma_n$  is estimated assuming  $\theta = 50^\circ$  and  $\sigma_3 \rightarrow \sigma_2$  (transpressional regime). These estimates yield a possible range of values of  $\lambda$  between 0.7 and 1.8 for the transtensional and transpressional conditions, respectively.

[11] If the coseismic damage lowers the effective shear modulus of the fault zone but does not affect the Poisson's ratio ( $\delta\nu = 0$ ), from equation (10) one can see that the fault zone will subside if  $\lambda < (1-\nu)/\nu$ . In particular, this implies  $\lambda < 3$  for a Poisson solid ( $\nu = 0.25$ ) and  $\lambda < 1$  for an

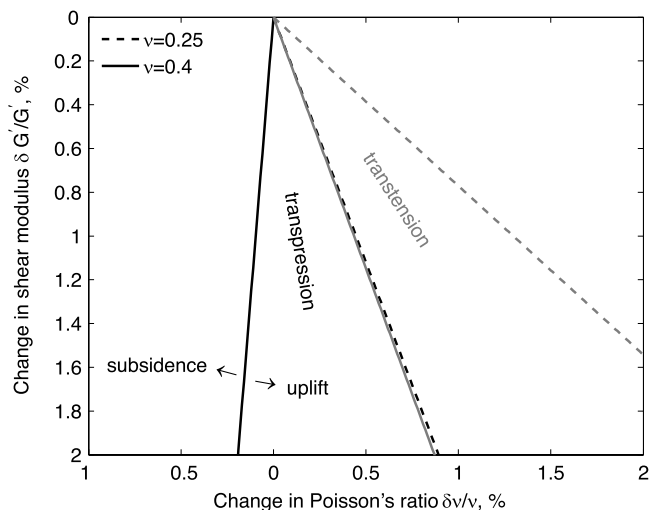


**Figure 4.** Sign of vertical displacement as a function of changes to  $\nu$  and  $G$ , from analytical solutions. Solid black line shows boundary between CZ uplift and subsidence for transpression with  $\lambda = 1.8$ , and  $\nu = 0.4$ . Solid grey line shows this boundary for transtension ( $\lambda = 0.7$ ). The dashed lines show these boundaries for compliant zones with  $\nu = 0.25$ . All calculations assume rock density  $\rho_r = 2.6 \times 10^3 \text{ kg m}^{-3}$  and coefficient of friction  $\mu = 0.6$ .

incompressible solid ( $\nu \rightarrow 0.5$ ). If the Poisson's ratio of fault damage zones is close to 0.25, coseismic softening will always be accompanied by subsidence. Such gravity-driven subsidence scales as  $\delta u_3 \sim \rho_r g l^2 \delta G'/G'^2$ , where the length scale  $l$  corresponds to the fault zone width  $2w$  or depth  $h$ , whichever is smaller. For a reasonable range of parameters the predicted gravitational subsidence may be as large as a few tens of centimeters, greatly exceeding the elastic response of compliant zones to the coseismic stress changes, as well as the observed magnitudes of vertical deformation around inferred fault zones [Fialko *et al.*, 2002; Fialko, 2004; Hamiel and Fialko, 2007]. However, for higher Poisson's ratios there exists a plausible range of fault-normal stresses that might offset vertical deformation due to the gravitational collapse ( $\lambda > 1$ ).

[12] Figure 4 illustrates the effects of changes in both  $G'$  and  $\nu$  on vertical deformation due to a damage zone. Lines in Figure 4 represent solutions for vanishing vertical deformation,  $\delta \varepsilon_{33} = 0$ , and demarcate regimes of contraction and subsidence (to the left of the lines) and expansion and uplift (to the right of the lines), as illustrated for a particular case of  $\nu = 0.4$  and high fault-normal stress (see black solid line in Figure 4). Solid lines in Figure 4 correspond to an initial fault zone  $\nu$  of 0.4, and dashed lines correspond to an initial  $\nu$  of 0.25. Black lines correspond to a transpressional regime ( $\lambda = 1.8$ ) and gray lines correspond to a transtensional regime ( $\lambda = 0.7$ ). High Poisson's ratios and fault-normal stresses indeed tend to counteract compaction due to gravity, and in fact may reverse the polarity of vertical deformation.

[13] These results indicate that the net vertical deformation due to a compliant fault zone may not be necessarily dominated by the gravitational collapse, and under certain conditions may be controlled by the coseismic stress

changes even in the presence of coseismic damage and softening of rocks comprising the fault zone.

### 3. Numerical Models

[14] To gain a further quantitative insight into deformation of compliant fault zones due to the Landers and Hector Mine earthquakes, we perform finite element (FE) simulations that account for contributions from the coseismic stress changes, coseismic softening of the fault zones, and regional stress. To model the Landers and Hector Mine coseismic stresses, we use a large FE model incorporating the Landers and Hector Mine ruptures and several compliant zones, which we will refer to as the “ensemble model.” This model, and finer-scale models of individual compliant zones, are used to compute the total elastic strain within the fault zones and their immediate surroundings. Both model meshes incorporate the same elastic structure, as described in section 3.1. We use the finite element code GAEA [Saucier and Humphreys, 1993] to perform these calculations.

#### 3.1. Elastic Structure

##### 3.1.1. Elastic Properties of the Mojave Crust and Compliant Zones

[15] We infer elastic properties of the compliant zones and the surrounding crust from seismic velocities ( $V_p$  and  $V_s$ ) and assumed rock density. Given  $V_s$  in the Landers compliant zone [Li *et al.*, 1999] and assuming a density of  $2500 \text{ kg/m}^3$ , the shear modulus  $G$  should be about 2.5 GPa in the top kilometer, increasing to 10 GPa below 1 km depth and to 16 GPa below 8 km depth. Li *et al.* obtain  $G = 8 \text{ GPa}$  for the country rock surrounding the fault zone at 0 to 1 km depth, a value which is significantly less than the value for 0 to 2 km depth in the Jones and Helmsberger [1998] elastic model (13 GPa). For the compliant zone along the Landers earthquake rupture (Johnson Valley Fault, or JVF), Li and Vidale [2001] estimate that  $\nu$  is relatively high ( $\nu = 0.34$ ). This is consistent with laboratory data and other seismic observations, which indicate that accumulation of damage increases the effective Poisson's ratio of rocks [e.g., Li *et al.*, 2006; Faulkner *et al.*, 2006]. Table 1 summarizes the 1-D elastic structure we used to model the CZs and the surrounding crust in both the regional-scale and individual CZ models. We consider two “end-member” cases of the Poisson ratio of the compliant zones of  $\nu = 0.25$  and  $\nu = 0.40$ . The surrounding crust is assumed to have a constant value of  $\nu = 0.25$ . Uniform elastic models were also developed, for comparison with analytical solutions. In these models, the Young's modulus  $E$  and the shear modulus  $G$  are 100 and 40 GPa (50 and 20 GPa in the compliant zones), which correspond to  $\nu = 0.25$ .

**Table 1.** Layered Elastic Model<sup>a</sup>

Depth (km)	CZ $E'$	CZ $G'$	Host Rock $E$	Host Rock $G$
0–1	10	4	20	8
1–2	18	7.2	35	14
2–5	35	14	70	28
5–32	80	32	80	32
32+	170	68	170	68

<sup>a</sup>Test models only.  $G$  and  $E$  units are GPa. For the models, the elastic constants for 1–2 km were upward continued to the surface;  $\nu$  is 0.25, except in the indicated models with compliant zone  $\nu = 0.4$ .

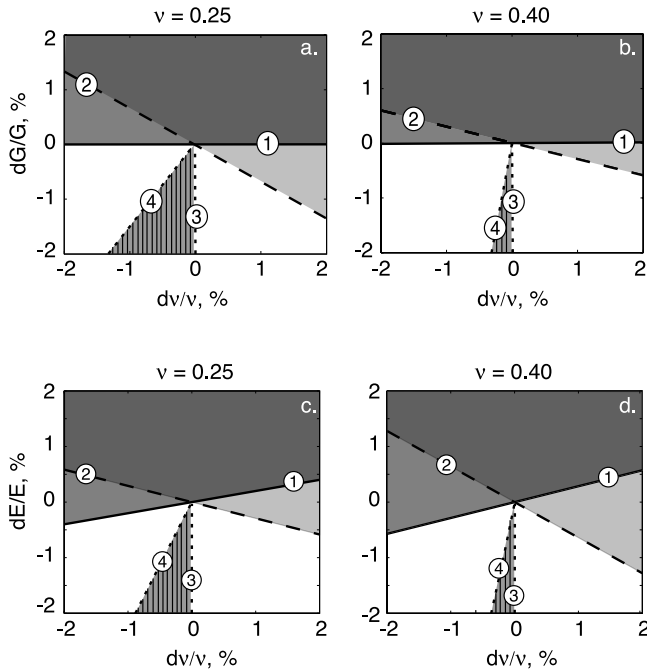


**Figure 5.** Admissible ranges of elastic parameters, based on the observations of *Vidale and Li* [2003]. (a and b) Admissible ranges of  $\partial G/G$  and  $\partial \nu/\nu$ , for direct comparison with the parameter space on Figure 4. (c and d) Admissible ranges of  $\partial E/E$  and  $\partial \nu/\nu$  for the FE models. Line 1 separates regions where  $V_s$  increases (shaded) from regions where it decreases. Line 2 separates areas where  $V_p$  increases (shaded) from regions where it decreases. Line 3 defines where  $R = 1$ . Line 4 defines where  $R = 0.7$ . The region marked with vertical lines is where both  $V_p$  and  $V_s$  decrease coseismically, with  $0.7 < (\partial V_s/V_s)/(\partial V_p/V_p) < 1$ .

### 3.1.2. Coseismic Changes to Compliant Zone Elastic Parameters

[16] In our numerical models, coseismic changes to compliant zone elastic properties are constrained by observations from the Johnson Valley Fault [*Vidale and Li*, 2003]. *Vidale and Li* [2003] observed that both  $V_p$  and  $V_s$  in the top few kilometers of the Johnson Valley Fault (JVF) compliant zone fell by about 0.5% following the Hector Mine earthquake. Figure 2 of *Vidale and Li* [2003] shows that the percentage drop in  $V_s$  ( $\partial V_s/V_s$ ) was between about 70 and 100% of the percentage drop in  $V_p$  ( $\partial V_p/V_p$ ). Using this information, we can limit the range of elastic parameter values to model. GAEA requires as input elastic parameters  $E$  and  $\nu$ , so we define admissible ranges of these parameters here. We do the same for  $G$  and  $\nu$  so the admissible parameter range may be compared with that shown in Figure 4. Perturbations in the elastic moduli  $\partial E$  and  $\partial \nu$  are related to the observed perturbations in seismic velocities as follows:

$$\partial V_s = \frac{\partial V_s}{\partial E} \partial E + \frac{\partial V_s}{\partial \nu} \partial \nu < 0 \quad (11)$$

$$\partial V_p = \frac{\partial V_p}{\partial E} \partial E + \frac{\partial V_p}{\partial \nu} \partial \nu < 0. \quad (12)$$

Defining  $R$  as the ratio of coseismic changes in  $V_s$  and  $V_p$ , we come up with a narrower constraint:

$$R = \frac{\partial V_s/V_s}{\partial V_p/V_p} \quad (13)$$

$$0.7 < R < 1. \quad (14)$$

Using well-known expressions for  $V_p$  and  $V_s$  in terms of  $E$  and  $\nu$ , we find that

$$R = \left[ \frac{\partial E}{2E} + \frac{\partial \nu}{\nu} \left( \frac{\nu}{2(1+\nu)} \right) \right] \left[ \frac{\partial E}{2E} + \frac{\partial \nu}{\nu} \left( \frac{4\nu^2(2-\nu)}{(1-\nu)} \right) \right]^{-1}. \quad (15)$$

Figure 5 shows the admissible ranges in  $\partial E/E$  and  $\partial \nu/\nu$ , assuming about a 0 to 2% drop in  $V_p$ . The shaded areas are parameter ranges for which  $V_s$  or  $V_p$  (or both) would increase coseismically. The hatched area is that for which equation (14) holds. Figure 5 shows that a decrease in  $E$  (which is required for both  $V_s$  and  $V_p$  to drop), must be accompanied by a constant or decreasing  $\nu$ . The range of admissible  $\partial \nu/\nu$  values is much narrower for the  $\nu = 0.4$  case than it is for the  $\nu = 0.25$  case. For these computations we assume that  $G = 20$  GPa, meaning that for the  $\nu = 0.25$  case,  $E = 50$  GPa and for the  $\nu = 0.4$  case,  $E = 56$  GPa. We use a similar approach to define admissible ranges of  $\partial G/G$  and  $\partial \nu/\nu$ . This exercise shows that while  $G$  decreases (as it must, for  $V_s$  to drop),  $\nu$  must either decrease or remain constant.

[17] To reduce computation time, we model cases in which  $E$  (equivalently,  $G$ ) decreases by 1% and  $\nu$  does not change. This corresponds to a  $\sim 0.5\%$  decrease in both  $V_s$  and  $V_p$ , and  $R = 1$ . Note that because seismic data are available only for the Johnson Valley fault zone, the inferred constraints may not be applicable elsewhere.

## 3.2. Ensemble Model Incorporating Several Mojave Compliant Zones

[18] Our regional model of the Eastern California Shear Zone in the Mojave desert covers a 1000-km square area, to a depth of 300 km (Figure 6). In the area of the Landers and Hector Mine earthquake ruptures, as well as along the compliant zones, nodal spacing is 1 to 2 km, and the 20-node quadratic model elements are 2 km in dimension. Element dimensions increase away from the center of the model. Elements are 5 km deep in the upper crust, and increase in dimension with depth. In this coarse mesh, CZs are one model element (three nodes) wide. Boundary conditions are described in sections 3.1.1 and 3.1.2. The ensemble model is too coarse to model in detail the strain of individual compliant zones, but it allows us to investigate the deformation of multiple compliant zones together, that is, the extent to which they affect the stress field, and whether all Mojave CZs must be incorporated in our estimates of coseismic stress on individual CZs.

### 3.2.1. Coseismic Stress Change due to the Hector Mine Earthquake

[19] For the coseismic stress change models, the side and bottom boundaries of the ensemble model are fixed and the top boundary is stress-free. We used the smoothed Hector

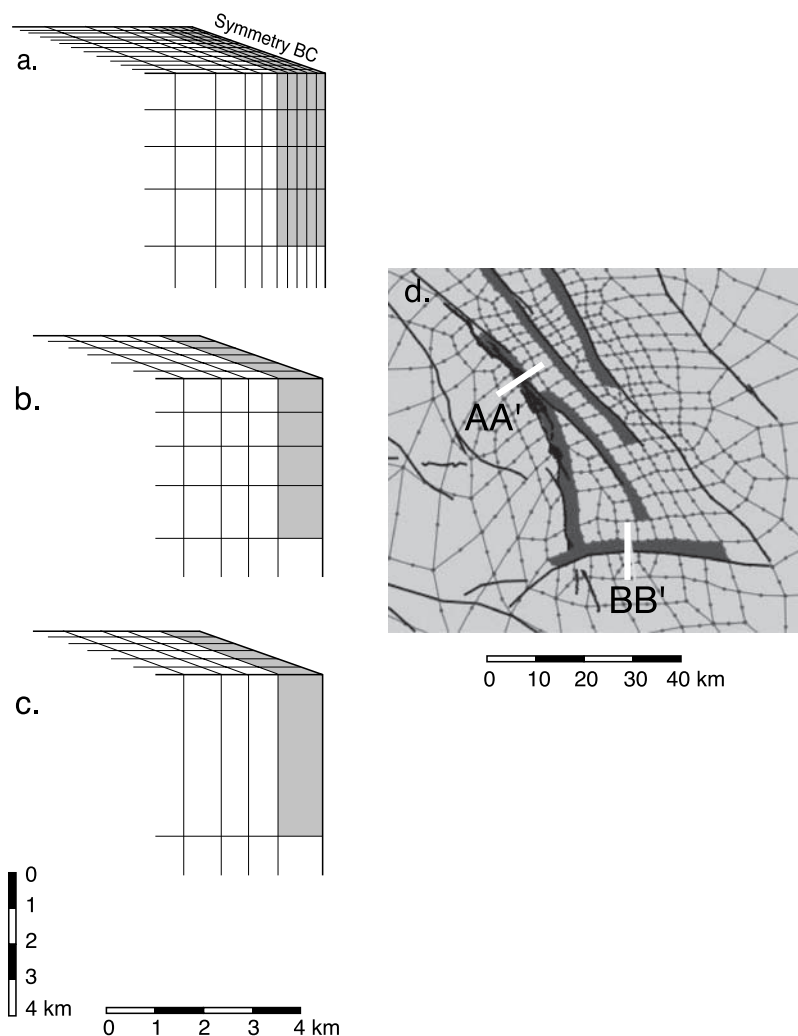


**Figure 6.** Representation of compliant zones in finite element meshes. (a) Mesh A is the detailed test mesh, and (b and c) meshes B and C are test meshes developed to assess sensitivity of results to element size. (d) The Mojave mesh with an ensemble of compliant zones (partly shown) has 5-km-deep elements in the top 20 km of the crust, gradually increasing in dimension with depth. Nodal spacing for all meshes is half of the element dimension: there are three nodes per element edge.

Mine rupture geometry from *Kaverina et al.* [2002], together with GPS coseismic displacements [*Agnew et al.*, 2002] to generate a slip distribution for the Hector Mine earthquake. This slip distribution, and its total moment, are very similar to that of *Simons et al.* [2002], except that all of the slip in our model occurs along a single, curved surface. The moment of the modeled slip ( $6.0 \times 10^{19}$  N m) falls within the range of geodetic and seismic moment estimates for the Hector Mine earthquake. Crustal stresses are fairly insensitive to the effects of elastic layering as long as the coseismic slip used in the stress modeling was derived with the same elastic structure [*Hearn and Bürgmann*, 2005].

### 3.2.2. Background Stress

[20] We assume that the maximum compressive principal stress  $\sigma_1$  in the Mojave Desert is oriented about N20°E [e.g., *Townend and Zoback*, 2004]. However, the average shear stress on faults in the Eastern California Shear Zone is uncertain. The coefficient of static friction,  $\mu$ , is not known (though it is suspected to be greater than for major plate-bounding faults [*Townend and Zoback*, 2004]). Parts of the

Mojave may be experiencing transtension [*Dokka et al.*, 1998; *Dokka and Macaluso*, 2001] while in other areas (i.e. the Mojave block), transpression may be dominant [*Bartley et al.*, 1990]. Given these uncertainties, we focus on end-member cases with  $\mu = 0$  and  $\mu = 0.7$ , and, for the latter friction value, we investigate three stress states. Table 2 shows values of principal stresses  $\sigma_1$ ,  $\sigma_2$  and  $\sigma_3$  for these stress scenarios. For  $\mu = 0$ ,  $\lambda = 1$  for all faults, and for  $\mu = 0.7$ ,  $\lambda = 0.9$  to 1.7, depending on fault orientation and whether transpression, pure shear, or transtension is assumed.

[21] To model appropriate background stress in the ensemble model, we imposed  $\sigma_{11}$ ,  $\sigma_{22}$  and  $\sigma_{12}$  by displacing model boundaries. In the ensemble model coordinates, the positive  $x_1$  direction is east, and the positive  $x_2$  direction is north. By scaling and superimposing these stress components, one may reproduce any relevant (2-D) deviatoric stress. Shear stresses acting on horizontal planes were assumed to be zero, that is,  $\sigma_{33}$  is assumed to be the intermediate principal stress at all depths. We model lithostatic stress by enabling gravitational body forces, which

**Table 2.** Anderson Stress States in the Mojave Region

$\mu$	$\theta_o^a$	$\theta_l^b$	$\sigma_1^c$	$\sigma_2^c$	$\sigma_3^c$
0.0 <sup>d</sup>	45	90	20	20	20
0.7 <sup>e</sup>	28	56	26	26	14
0.7 <sup>f</sup>	28	56	35	26	17
0.7 <sup>g</sup>	28	56	69	26	26

<sup>a</sup>The parameter  $\theta_o$  is optimal slip angle in degrees.

<sup>b</sup>The parameter  $\theta_l$  is lockup angle in degrees.

<sup>c</sup>Stresses are in MPa per km depth.

<sup>d</sup>Case 1, low friction, all stress states.

<sup>e</sup>Case 2, high friction, transension.

<sup>f</sup>Case 2, high friction, pure shear.

<sup>g</sup>Case 2, high friction, transpression.

results in a depth-dependent, vertical compressive stress and horizontal compressive stresses that scale with the vertical stress ( $\sigma_{33}/3$ , for  $\nu = 0.25$ ). Lithostatic stress is then represented using a superposition of horizontal loads and deformation due to gravity. For layered elastic models, the boundary conditions are adjusted to cause an approximately linear increase in deviatoric stress with depth (as required to ensure a constant friction coefficient). To compute CZ strain in response to coseismic softening, we ran models with two different values of  $E$  in the compliant zone, and differenced the results.

### 3.3. Fine-Scale, Single CZ Models

[22] We model details of CZ deformation, and assess sensitivity of model results to nodal spacing, using a finer, more regular mesh (Figure 6). The coordinate system for this mesh, which incorporates a single CZ, is the same as that used in section 2 (Figure 3). Horizontal and vertical nodal spacing in the CZ are 100 m and 250 m, respectively. Elements gradually coarsen with depth and away from the CZ. Since we are interested only in short-wavelength deformation, the modeled domain is a 50 km cube. The CZ falls along one side of this cube so we can take advantage of the problem's symmetry (with an appropriate choice of boundary conditions). Deviatoric stresses are imposed by displacing the side model boundaries. Lithostatic stress, and CZ strain in response to coseismic softening, are both modeled as described for the ensemble model (above).

## 4. Results of Finite Element Simulations

### 4.1. Ensemble Model: Hector Mine Earthquake

#### 4.1.1. Coseismic Stress Change and the Response of Compliant Zones

[23] The first question we address with the ensemble model is how CZs affect coseismic stress changes. That is, if we ignore, or assume a particular distribution of CZs, does this influence estimates of coseismic stresses acting on individual compliant zones?

[24] Figures 7a and 7b show how 10-km-deep CZs affect coseismic shear and normal stresses resolved onto surfaces parallel to the Pinto Mountain Fault (PMF) and the Camp Rock Fault (CRF). As one might expect, compliant zones may perturb the stress field locally. For example, a local concentration of strain resulting from the collapse or expansion of a CZ can affect normal stresses in the host rock around and beyond its ends. Figure 7 also shows that at

transects AA' and BB' across the CRF and PMF compliant zones, the computed stresses are fairly insensitive to the presence of other CZs and therefore to the specific configuration of CZs in our ensemble model. Differences in computed stress components are of the order of 10% or less, which is acceptable for our purpose. Overall, shear and normal stresses resolved onto the PMF and the CRF at the profile locations are similar to those obtained by *Fialko et al.* [2002], though these stresses vary greatly with position in the vicinity of the CRF profile.

[25] Figure 8 shows profiles of predicted coseismic line of sight (LOS) displacements across the PMF and the CRF, due to stress changes from the Hector Mine earthquake, together with InSAR data. The modeled displacement profiles are qualitatively similar to the InSAR data. The Hector Mine earthquake caused a negative LOS displacement (an increase in radar range) across the PMF, principally from subsidence of the compliant zone. These negative LOS displacements are underestimated by the model, in part because of the coarse discretization of the

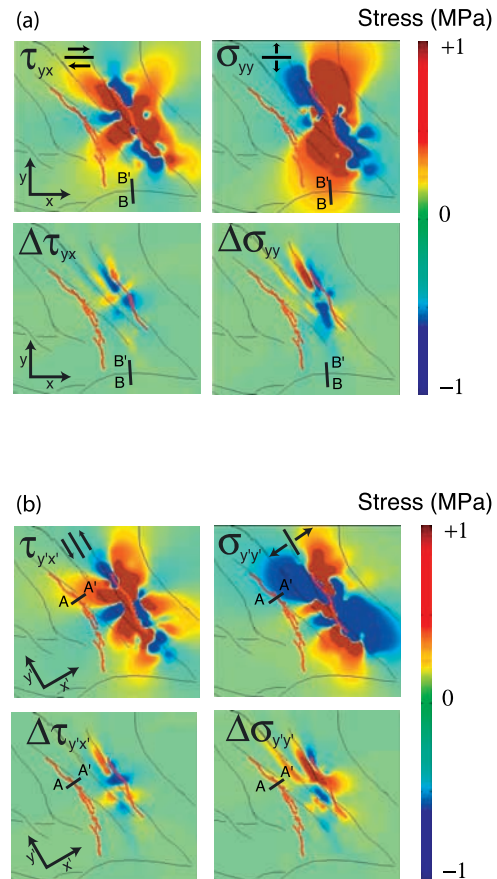


**Figure 7.** (a) Effect of compliant zones on the Hector Mine earthquake coseismic stress field. (top) Hector Mine earthquake coseismic shear and normal stresses resolved onto planes parallel to the Pinto Mountain Fault. The model used to compute these stresses includes the compliant zones shown on Figure 6d, extending to a depth of 10 km. (bottom) Residuals (these stresses minus stresses from a model without compliant zones). (b) The same quantities as in Figure 7a, with the shear and normal stress components resolved onto planes parallel to the Camp Rock Fault.

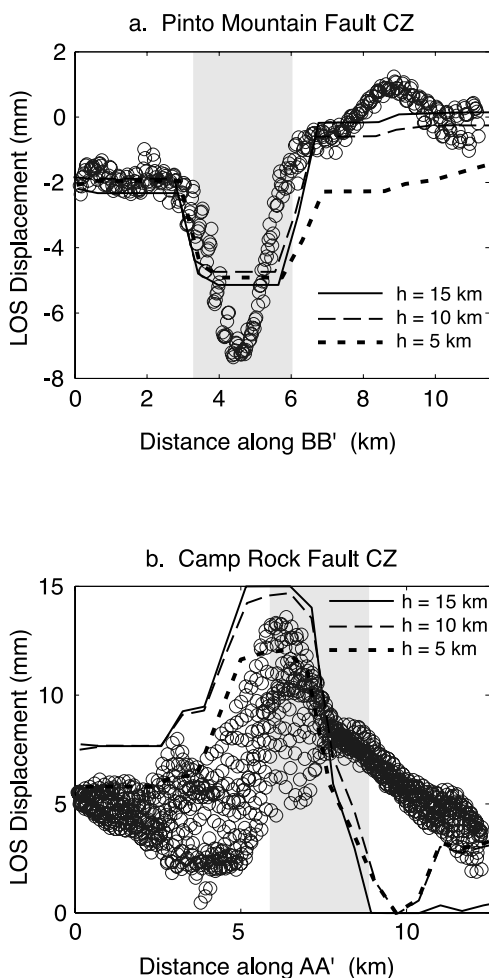


**Figure 8.** Compliant zone strain due to Hector Mine earthquake coseismic stress change, from the ensemble mesh. (a) Modeled line-of-sight (LOS) displacements along profile BB' (traversing the profile from south to north). (b) LOS displacements along profile AA', traversing the profile from west to east. The LOS displacements are in the direction (0.38,  $-0.09$ , 0.92) in (east, north, up) coordinates.

ensemble mesh. Across the CRF, the Hector Mine earthquake caused fault-normal contraction and left-lateral shear, resulting in a negative slope in the LOS displacement profile (Figure 8). The modeled slope exceeds that indicated by the InSAR data. CZ strain due to coseismic stresses is only modestly sensitive to the compliant zone depth, particularly in the case of subsidence resulting from fault-normal tension. Shear across the CZ is also modestly dependent on depth, when the latter exceeds the CZ width. For example, an increase in CZ depth from 5 km to 15 km causes just a 50% increase in shear strain across the CRF.

#### 4.1.2. Response of Coseismically Softened CZs to Background Stress

[26] Figure 9 shows how the coseismically softened PMF and CRF compliant zones respond to background (lithostatic plus deviatoric) stress. Both CZs contract under the lithostatic stress, resulting in subsidence at the surface, CZ-normal shortening, and extension in the surrounding crust.

Vertical displacements due to the CZ appear to have two characteristic wavelengths: one of the order of the fault zone width (2 km), and the other of the order of the fault zone depth (5 km; Figures 9a and 9b). The region bounding the softened fault zones subsides by 10 to 20 mm with respect to the rest of the computational domain. For a given CZ width, the amplitude of this regional subsidence scales with the assumed depth of the CZ. We note that for extreme lithostatic contraction of a compliant zone, changes in stresses in the surrounding host rock could be significant relative to the coseismic stress change. In this case, the distribution of compliant zones would be central to generating estimates of coseismic stress on Mojave faults. However, the LOS displacement profiles on Figure 9 show that such contraction must be insignificant, meaning that the effect of lithostatic CZ contraction on stresses in the upper crust is small.

[27] Deviatoric stresses deform both the PMF and the CRF compliant zones far less than the lithostatic stress (Figures 9c and 9d). There is some uplift across the PMF CZ as it is at a high angle to the maximum compression axis  $\sigma_1$ . Right-lateral shear strain dominates the CRF CZ, resulting in a LOS displacement profile which is broadly consistent with InSAR data. For both compliant zones, the sign of strain due to softening under background deviatoric stress is opposite to that due to stress changes caused by the Hector Mine earthquake. This deformation is swamped by the lithostatic subsidence (Figures 9e and 9f), and its contribution to the coseismic strain (and hence, stress) field is modest. Since the effects of compliant zones on the coseismic stress field appear to be minor, we use stresses from our Hector Mine earthquake model (Figure 7) and the Landers earthquake elastic model of *Fialko* [2004] in our single-compliant zone models.

## 4.2. Finer-Scale, Single CZ Models

### 4.2.1. Test Models: Sensitivity to Nodal Spacing and Elastic Layering

[28] The displacement profiles on Figure 10 illustrate CZ deformation resulting from different stress components acting on a CZ which has softened by 10%. The CZ is 5 km deep and 2 km wide ( $h = 5$  km and  $w = 1$  km). The elastic properties and model dimensions are as given in section 3.1 and Table 1.  $E$  values for the layered models are scaled up so the top layer has the same  $E$  as the uniform half-space (UHS) model to facilitate comparisons among solutions.

[29] Figure 10a shows that shear stress acting parallel to the CZ yields enhanced shear strain within the CZ, and shear in the reverse sense outside of CZ. Instantaneous stresses resulting from gravitation, with horizontal stresses equal to 1/3 of the vertical stress, cause subsidence within and around the softened CZ, over a region whose dimension scales with its depth (Figure 10b). Compressive, uniaxial normal stress yields fault-normal contraction in the CZ and extension outside the CZ (Figure 10c). This results in subsidence on either side of the softened CZ, and uplift within the CZ (Figure 10d).

[30] To test the effect of mesh discretization on our calculations, we model CZ deformation in response to shear and normal stresses, using coarser FE meshes (meshes B and C on Figure 6). Coarser discretization in the horizontal

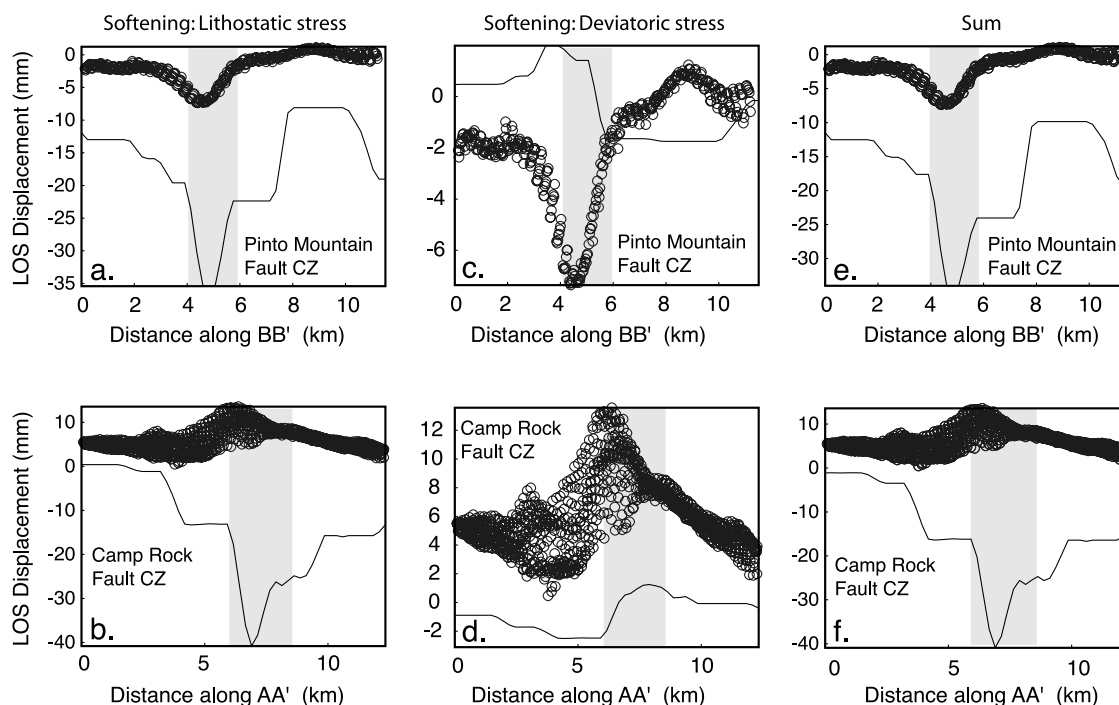


**Figure 9.** Compliant zone strain due to coseismic softening, from the ensemble mesh. (a and b) LOS displacements due to compliant zone compaction under lithostatic stress (which leads to subsidence). (c and d) LOS displacements due to compliant zone strain resulting from the deviatoric stress. (e and f) LOS displacements due to both lithostatic and deviatoric stress. The lithostatic stress contributes more to LOS displacements than the deviatoric stress, or the coseismic stress change (Figure 8). The step in profile BB', north of the PMF (Figures 9a and 9c) results from subsidence of the modeled Emerson Fault compliant zone, which is northeast of the BB' transect (Figure 6).

dimension (mesh B), has a limited effect on the CZ deformation in response to normal stresses (Figures 10b, 10c, and 10d) and a negligible effect on the results for fault-parallel shear stress (Figure 10a). As expected, coarse meshes with a single element representing the entire depth of the CZ only crudely represent the deformation.

[31] We also examine the effect of varying the layered elastic structure on CZ strain. Horizontal CZ strain resulting from shear and normal stresses is not strongly affected by the layered structure (Figures 10a and 9c). Vertical displacements due to gravitational body forces or fault-normal stresses are about 20% higher in the layered models than in UHS models with identical elastic properties of the top layer.

[32] For the UHS models, results shown in Figure 10 may be compared with the plane strain and antiplane strain analytical solutions in section 2. Displacement across the modeled CZ in response to an applied shear stress of 80 MPa acting on a CZ with  $E = 50$  GPa (i.e.,  $G = 20$  GPa), a 10% coseismic drop in  $E$ , and  $\nu = 0.25$ , matches the analytical solution (250 mm across half of the 2-km-wide CZ, see Figure 10a). Horizontal and vertical displacements of a CZ under a uniaxial normal stress of 200 MPa are somewhat less than plane strain analytical solutions. The analytical solutions give 0.38 m of contraction across half of the CZ (compared with 0.3 m from the FE model) and 0.25 m of uplift (compared with about 0.17 m for the FE model, with some of this outside the CZ; Figures 10c and 10d). These differences likely arise because the host rock exerts

tractions on the bottom and sides of the CZ in the finite element models. Our numerical estimate of vertical displacements due to the lithostatic load of 20 MPa/km (subsidence of 100 mm, Figure 10b) is also in agreement with the plane strain analytical solution (equation (10) in section 2), if we choose  $x_3 = 2500$  m ( $h/2$ ) and integrate this (mean) strain for  $x_2 = 0$  to  $w$ .

#### 4.2.2. Effect of Variations in $\nu$

[33] In this study, we have chosen to vary  $E$  (equivalently,  $G$ ), while holding  $\nu$  constant. This is justified by the tight constraint on coseismic changes in  $\nu$  (Figure 5 and section 3.1.2). However, the trapped wave velocity data permit a small coseismic reduction in  $\nu$ .

[34] Rather than investigate all such models, we ran a set of test models, varying  $\nu$  and holding  $E$  constant ( $E$ , and not  $G$ , is specified in input files for the finite element modeling code). Coseismically dropping  $\nu$  affects CZ shear deformation in the same way as coseismically increasing  $G$ . This is expected from the definition of  $G$  in terms of  $\nu$  and  $E$ . Decreasing  $\nu$  also amplifies CZ subsidence under lithostatic stress (as decreasing  $\nu$  causes a reduction in  $K$ ), and it suppresses CZ vertical displacements under uniaxial stress normal to the compliant zone. In summary, models in which both  $E$  and  $\nu$  decrease would suppress deviatoric strain and enhance lithostatic subsidence relative to the models we present. Coseismically increasing  $\nu$  does the opposite, that is, strain of a softened compliant zone under deviatoric stress is enhanced and its subsidence under lithostatic pressure is suppressed. Given the narrow limits on  $\partial\nu/\nu$

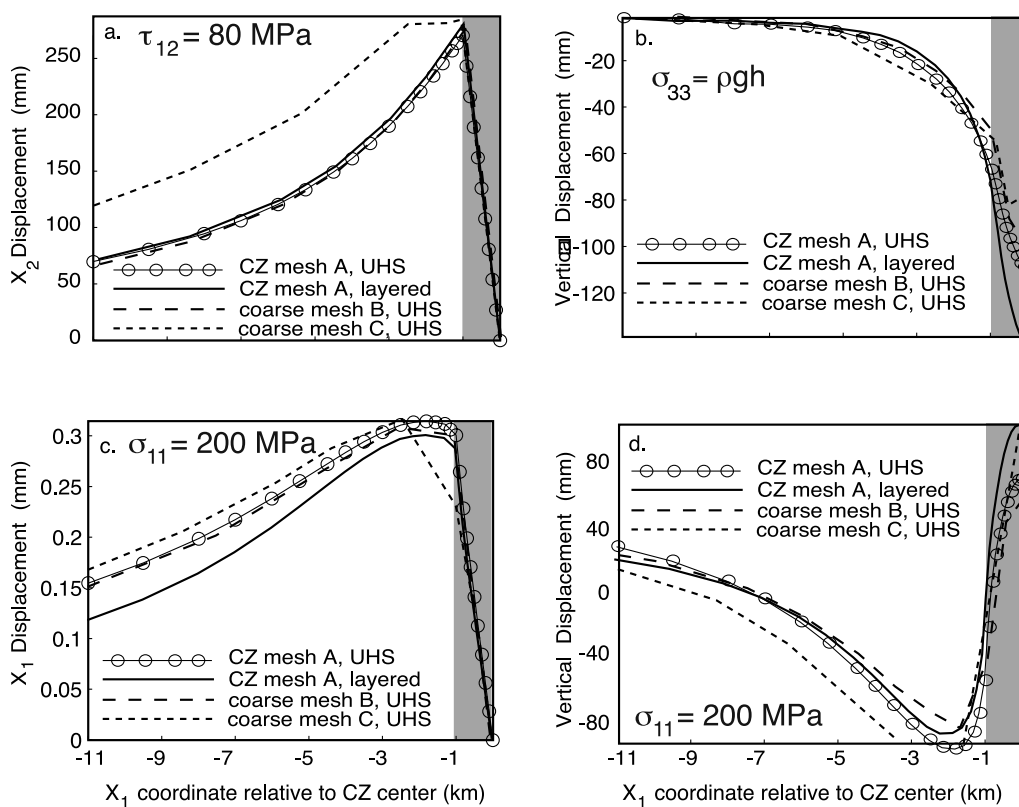


**Figure 10.** Sensitivity of modeled compliant zone deformation to model node spacing and layered elastic structure. These results are for single-compliant zone models, using meshes A, B, and C (shown on Figure 6). (a) The modeled horizontal displacements resulting from a shear stress of 80 MPa. (b) Modeled vertical displacements resulting from weight of the rock column:  $\sigma_{33}$  is 20 MPa per km depth and the horizontal normal stresses are 1/3 of this. (c and d) Modeled CZ-normal horizontal and vertical displacements due to a horizontal normal stress of 200 MPa. Coordinates are the same as those used in section 2 (and shown in Figure 3). The compliant zone's  $E$  is 10% less than that of the host rock. For the layered model,  $E$  values are scaled so the top layer has the same  $E$  as the uniform elastic (UHS) model. In these models the compliant zone is 5 km deep and 2 km wide.

in Figure 5, especially for  $\nu = 0.4$  (the more likely value as described below), we consider the results presented here to be representative of compliant zones whose properties change coseismically like the Johnson Valley Fault.

#### 4.2.3. Coseismic Deformation of the Pinto Mountain Fault Compliant Zone

[35] We used the single-compliant zone model to examine how the CZ width, depth, and Poisson's ratio  $\nu$  affect the coseismic deformation of the Pinto Mountain fault zone during the Hector Mine and Landers earthquakes. LOS displacements across the PMF in response to the 1999 Hector Mine earthquake indicate local subsidence and a small component of right-lateral shear. This deformation must result from both coseismic stress change and (presumed) coseismic CZ softening. Figure 11 shows contributions to the LOS displacements from (1) the Hector Mine earthquake coseismic stress change (0.4 MPa of tension across the fault) (2) coseismic softening of the compliant zone, as well as (3) their sum. The total background stress is assumed to be consistent with  $\mu = 0.7$  and pure shear (Table 2).

##### 4.2.3.1. Maximum LOS Displacement

[36] Strain resulting from deviatoric background stress and coseismic CZ softening accounts for only about 1 to

6 mm of positive LOS displacement for models with CZ  $\nu = 0.25$ , and 2 to 7 mm of positive LOS displacement for models with CZ  $\nu = 0.4$ . For low  $\mu$  (or for transtension), lithostatic stress drives virtually all of the deformation (i.e. subsidence) due to CZ softening (Figures 11b and 11d). Transtension has been suggested for this region [e.g., Dokka *et al.*, 1998; Dokka and Macaluso, 2001].

[37] For the Hector Mine earthquake, the acceptable range of maximum LOS displacements for the PMF is 6 to 8 mm [Fialko *et al.*, 2002]. The cross-hatched regions on Figures 11c and 11f indicate a range of CZ dimensions which are compatible with these data. If the CZ is deep, it must be narrow to generate just 6 to 8 mm of subsidence, whereas a broader CZ is admissible if it is shallow. Compliant zones with either Poisson's ratio can be consistent with the observed subsidence. For  $\nu = 0.4$ , the coseismic stress change contribution is more important than the softening contribution. Also, if we assume no coseismic softening, a range of compliant zones (deeper and broader than the ranges in Figures 11c and 11f) may generate the observed subsidence (Figures 11a and 11d).

[38] Figure 12 shows model predictions for the coseismic uplift or subsidence of the PMF due to the 1992 Landers

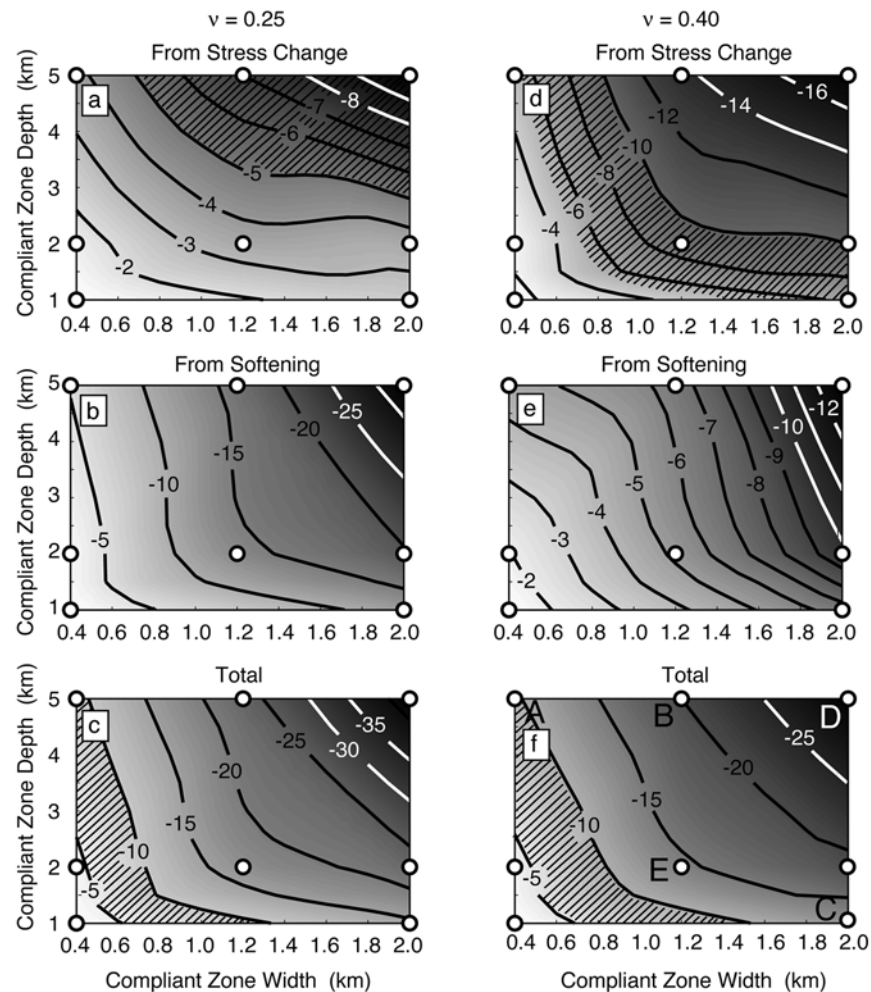


**Figure 11.** Sensitivity of PMF compliant zone deformation to geometry and Poisson's ratio, for the 1999 Hector Mine earthquake. (a, b, and c) Results for  $\nu = 0.25$ , and (d, e, and f) results for  $\nu = 0.4$ . Maximum, modeled LOS displacements from coseismic stress change (Figures 11a and 11d), softening (Figures 11b and 11e), and their sum (Figures 11c and 11f) are shown. Since the peaks and troughs in modeled LOS displacement profiles may be offset, the values shown in Figures 11a and 11d may not sum to those shown in Figures 11c and 11f. Most of the LOS displacement may be attributed to uplift (for positive LOS displacements) or subsidence (negative LOS displacements). Hatched regions show where the LOS displacement is consistent with InSAR observations [Fialko *et al.*, 2002]. In these models, the compliant zone E is 50% of the host rock value and drops a further 1% coseismically. Letters refer to models for which LOS displacement profiles are shown on Figure 13.

earthquake. The Landers earthquake caused 0.4 MPa of right-lateral shear and 0.6 MPa of fault-normal compression at the PMF transect location [Fialko, 2004], which should cause right-lateral shear and uplift of the PMF CZ. The effect of the fault zone softening is mostly subsidence under the lithostatic load, exactly as for the Hector Mine earthquake. The summed vertical displacement of the CZ must be about 2 cm of uplift (Figure 13d), so the range of admissible models is more narrowly defined than for the Hector Mine earthquake. None of the models incorporating both the coseismic softening and stress change contributions can generate two centimeters of uplift. Figure 12d shows that this is possible for some compliant zones if there is no coseismic softening of the PMF. A deeper (10-km-deep, 2-km-wide) CZ can generate 2 cm of uplift with both the

softening and the stress change terms, though the rest of the LOS displacement profile does not match observations (see below and Figure 13b).

#### 4.2.3.2. Modeled LOS Displacement Profiles: The Relative Contributions of Coseismic Stress Change and Softening

[39] Figures 13a and 13b show profiles of modeled LOS displacements across the PMF, for the Hector Mine and Landers earthquakes. All of the compliant zones yield too much subsidence in response to the Hector Mine earthquake, with the exception of model A (400 m wide, 5 km deep). Figure 13b illustrates that depending on the CZ dimensions, the combination of coseismic stress due to the Landers earthquake and softening under total stress can yield either uplift or subsidence. In models with an

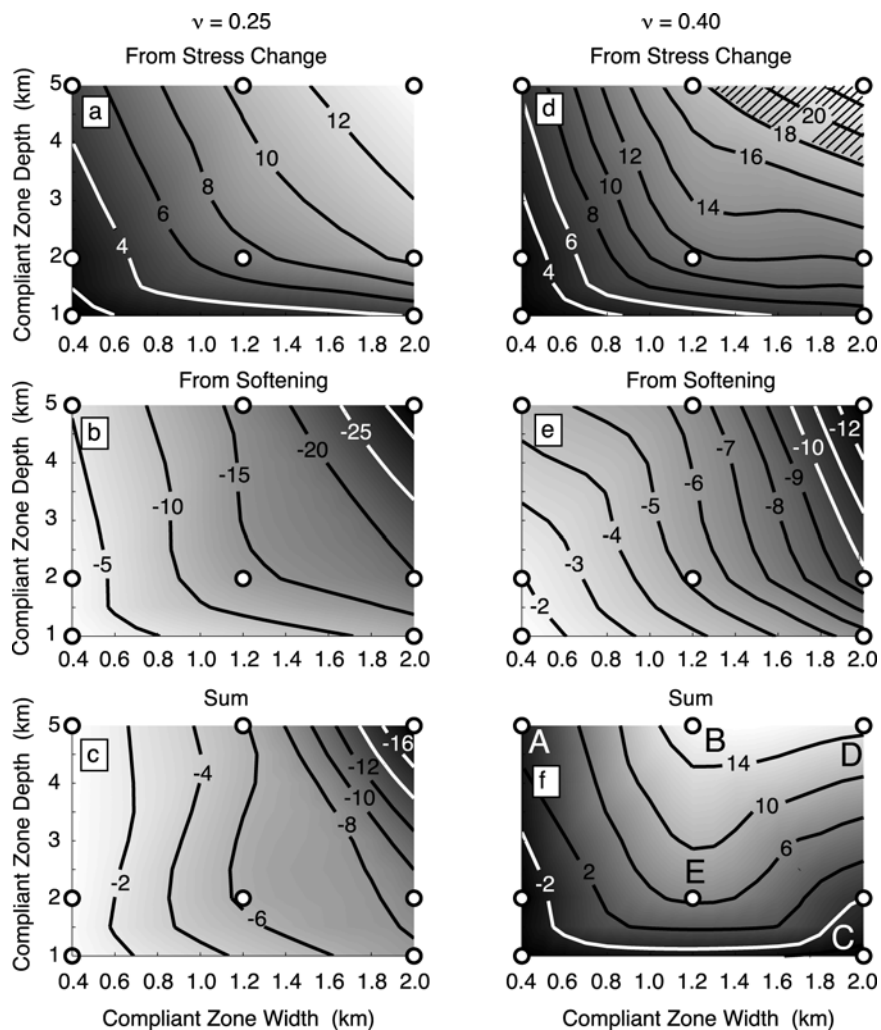


**Figure 12.** Sensitivity of PMF compliant zone deformation to geometry and Poisson's ratio, for the 1992 Landers earthquake. (a, b, and c) Results for  $\nu = 0.25$ , and (d, e, and f) results for  $\nu = 0.4$ . Maximum, modeled LOS displacements from coseismic stress change (Figures 12a and 12d), softening (Figures 12b and 12e), and their sum (Figures 12c and 12f) are shown. Since the peaks and troughs in modeled LOS displacement profiles may be offset, the values shown in Figures 12a and 12d may not sum to those shown in Figures 12c and 12f. Most of the LOS displacement may be attributed to uplift (for positive LOS displacements) or subsidence (negative LOS displacements). Hatched regions show where the modeled LOS displacement is consistent with InSAR observations [Fialko, 2004]. In these models, the compliant zone *E* is 50% of the host rock value and drops a further 1% coseismically. Letters refer to models for which LOS displacement profiles are shown on Figure 13.

uplifted CZ, the peak sits within a longer-wavelength depression caused by lithostatic contraction of the CZ. (Subsidence shown on Figure 13b is smaller than that shown on Figure 9 because here we assume  $\nu = 0.4$ .) Superimposed on the troughs in Figure 13b is a small amount of horizontal contraction, which maps to a positive LOS displacement gradient across the CZ. The LOS displacement data (Figure 13d), on the other hand, indicate uplift of about 2 cm and left-lateral shear across the CZ which maps to a negative LOS displacement gradient across the CZ. The InSAR LOS displacements on Figure 13d are the same as in Figures 8 and 9 and Figure 13 of Fialko [2004], though we note that the scale of the vertical axis in Figure 13 of Fialko [2004] is off by a factor of 2 due to a labeling error.

[40] Figures 13c and 13d illustrate how our PMF compliant zone models can fit the Hector Mine and Landers LOS displacement data, if we adjust the CZ rigidity and the percentage coseismic rigidity change. In general, we find that LOS displacement profiles may be modeled in this manner if lithostatic contraction is excluded. (Model C can approximately match the Hector Mine LOS displacement profile with softening (1% decrease in *E*) under total background stress (including lithostatic stress), but this model disallows any deformation due to the coseismic stress change, and it fails to explain the Landers earthquake LOS displacements.) Section 4 outlines some possible justifications for the negligible role of gravitational body forces in CZ deformation.

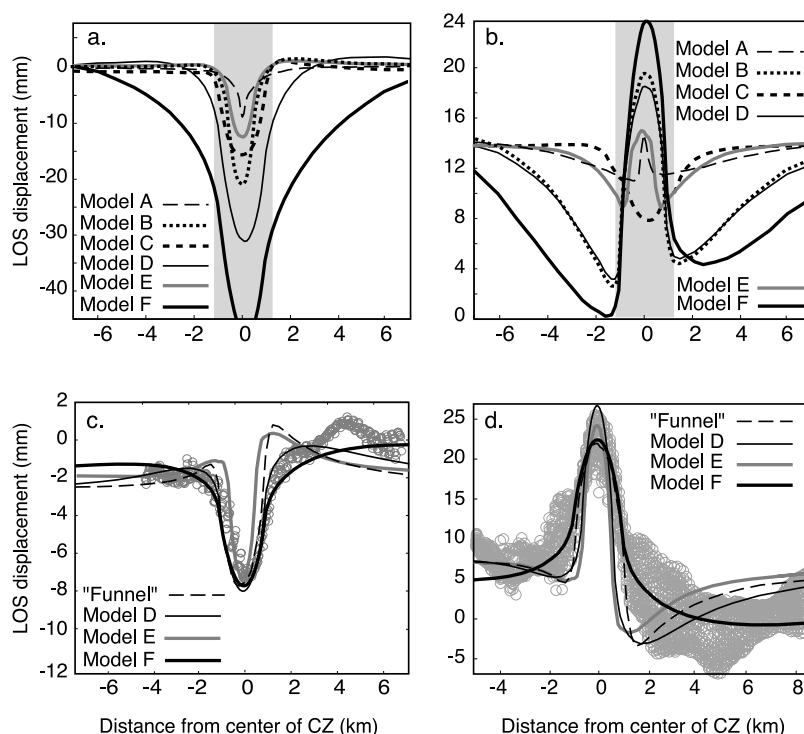


**Figure 13.** Modeled LOS displacement profiles for the Pinto Mountain Fault. A, B, C, D, and E refer to compliant zone models with the dimensions shown on Figures 11f and 12f, and with  $\nu = 0.4$ . Model F comprises a 10-km-deep, 2-km-wide compliant zone with  $\nu = 0.4$ . See text for a description of the “funnel” model. (a) Modeled LOS displacements for the Hector Mine earthquake, assuming that the CZ is 50% softer than the host rock and that it softens by another 1% coseismically. (b) Modeled LOS displacements for the Landers earthquake (same assumptions as for Figure 13a). (c) Model results which match the Hector Mine earthquake LOS displacements. This is achieved by assuming different softening properties and no lithostatic subsidence (see text). (d) Model results which match the Landers earthquake LOS displacements (see text). The LOS displacement data (gray circles) on Figures 13c and 13d are from *Fialko et al.* [2002] and *Fialko* [2004].

[41] The rigidity of the CZ relative to that of the host rock modulates the contribution of coseismic stress to the observed deformation. If this contribution must be scaled down to fit the LOS displacements, the CZ must be stiffer than we have been assuming in our models. The percentage decrease in  $E$  (or the magnitude of background deviatoric stress) modulates the contribution of coseismic CZ softening to the deformation. We are assuming a background stress state (Table 2), so if the softening contribution must be scaled up to fit the LOS displacements, we conclude that the CZ softened coseismically by more than 1%.

[42] With scaling of the coseismic stress and (deviatoric) softening terms, models C, D, E, and F can fit the observed LOS displacements across the PMF, for both the Hector Mine and Landers earthquakes. For model C, the CZ must be 50% softer than the host rock, softening coseismically by another 1% (9% for the Landers earthquake). For models D and E, the CZ must be about 25 to 30% softer than the host rock, with 1 to 3% coseismic softening. For model F, the CZ may be about 15 to 20% softer than the host rock, and 0 to 1% coseismic softening is required.

[43] Results from a model of a “funnel-shaped” compliant zone, inspired by the results of damage rheology models of fault system generation [*Finzi et al.*, 2009], are shown on

Figures 13c and 13d. In this model, the CZ is 2 km wide in the top kilometer of the crust, and it narrows to a width of 400 m at 2 km depth and below. Results from the “funnel” model and model C are very similar, so the model C results are not shown on Figures 13c and 13d.

[44] For nearly all of the CZ models on Figures 13c and 13d, a background stress state consistent with pure shear ( $d\sigma_n/dz = 7$  MPa/km,  $d\tau/dz = -6$  MPa/km) is more consistent with the LOS displacements than transtension. Transtension ( $d\sigma_n/dz = 0.75$  MPa/km,  $d\tau/dz = 2$  MPa/km) is preferable for the shallow CZ (model C).

#### 4.2.4. Coseismic Deformation of the Camp Rock Fault Compliant Zone

[45] Figures 14a and 14b show modeled profiles of LOS displacement across the Camp Rock Fault during the Hector Mine earthquake. As with the PMF, if we take into account the coseismic stress contribution and both the lithostatic and deviatoric softening contributions, none of the models yields LOS displacements which match observations. Lithostatic subsidence dominates, regardless of whether transpression or pure shear is assumed. (For pure shear,  $\sigma_n = 1.6$  MPa/km and  $\tau = -9.0$  MPa/km, and for transpression,  $\sigma_n = 21.2$  MPa/km and  $\tau = -17.7$  MPa/km.)

[46] Figure 7 shows that the Camp Rock Fault compliant zone experienced coseismic contraction and positive shear

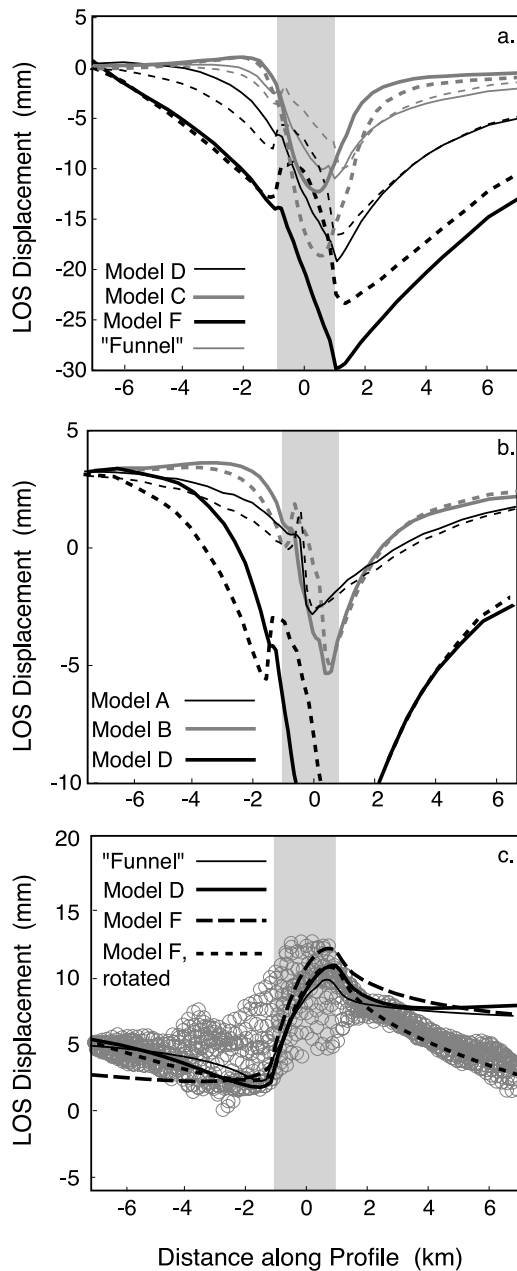


Figure 14

**Figure 14.** Modeled LOS displacement profiles for the Camp Rock Fault. A, B, C, and D refer to compliant zone models with the dimensions shown on Figures 11f and 12f, and with  $\nu = 0.4$ . Model F comprises a 10-km-deep, 2-km-wide compliant zone with  $\nu = 0.4$ . (a and b) Modeled LOS displacements for the Hector Mine earthquake, assuming that the CZ is 50% softer than the host rock, and that it softens by another 1% coseismically. Dashed lines show results for transpression, and solid lines show results for pure shear. Results for a “funnel” model, in which the CZ width tapers with depth, are also shown on Figure 14a (see text). (c) Model results which match the observed LOS displacements. This is achieved with different softening properties and no lithostatic subsidence (see text). The LOS displacement data (gray circles) on Figure 14c are from Fialko [2004].

stress (which would cause left-lateral shear strain across the CRF CZ) during the Hector Mine earthquake. The InSAR LOS displacement data suggest that this CZ contracted and was extruded upward, but that it sheared in a right-lateral sense, opposite to the coseismic strain. (Right-lateral strain across the CRF leads to a positive LOS displacement gradient across the CZ as shown on Figure 14c.) The sense of shear across the CRF compliant zone suggests that the background stress, and hence softening of the CZ, is causing most of its coseismic strain.

[47] To fit the shear across the CRF compliant zone, and the negative slope in the LOS displacement profile on either side (Figure 14c), a relatively stiff compliant zone with considerable coseismic softening is required. For a 1-km-deep CZ (model C), the CZ must be just 5 to 15% softer than the host rock, and must soften by 1 to 4%. For a 5-km-deep CZ (model D) the CZ must be 10 to 15% softer than the host rock and must soften by 1 to 4%. For a 10-km-deep CZ (model F), the results for transpression and pure shear differ: for transpression, the CZ rigidity is comparable to the host rock rigidity and it softens coseismically by about 0.5%, and for pure shear, the CZ is 20% softer than the host rock and it softens coseismically by 4%. In the vicinity of the CRF, pure shear is compatible with more coseismic softening (and a greater strain contribution from background deviatoric stress) than transpression is. This is because for pure shear, the compressive normal stress acting on the CRF is much smaller, leading to less CZ uplift. For all of the models, the CRF CZ must be substantially stiffer than the PMF CZ, and more coseismic softening is required.

## 5. Discussion

### 5.1. Determining Absolute Stresses and Rigidity of the Upper Crust

[48] We have shown that background tectonic stress contributes to the coseismic deformation of some Mojave compliant zones, and that models of this deformation may yield estimates of this stress. If the dimensions and elastic properties of the compliant zone are known, we may estimate the strain contribution from coseismic stress change, and subtract this contribution from the observed strain. This will isolate the strain due to coseismic softening of the CZ. This contribution depends on background deviatoric stress and the percentage change in compliant zone rigidity. If we know the coseismic change to the CZs elastic parameters, we can estimate the deviatoric stress (i.e., the deviatoric stress gradient over the depth interval occupied by the compliant zone).

[49] Stress at seismogenic depths might be estimated if compliant zones extended into the middle crust without narrowing substantially. Our models show that compliant zones must be of the order of 2 km wide near the Earth's surface, but they poorly constrain the width as a function of depth. Damage-controlled fault evolution models suggest that compliant zones around active faults generally become much narrower (and stiffer) at depth, though broad compliant zones may extend to seismogenic depths in tensional step overs [Finzi *et al.*, 2009]. If this is so, compliant zones along extensional step overs (or in strongly transtensional settings) would be good targets for future studies.

[50] We have assumed a background stress state (transpression, pure shear, or transtension) and varied the CZ stiffness and the coseismic change to  $E$  to fit LOS displacement data. Regardless of how we modulate the compliant zone  $E$  (i.e., the amplitude of the strain due to coseismic stress), we find that a component from background deviatoric stress is required to fit LOS displacements from the Hector Mine and Landers earthquakes. This is most obviously the case for the CRF, where the sense of shear across the CZ is opposite to the coseismic strain. However, the background deviatoric stress is also required to explain why there is so much more uplift of the PMF in the Landers earthquake than there is subsidence in the Hector Mine earthquake. The coseismic changes in normal stress for these events were  $-0.4$  MPa and  $0.6$  MPa, respectively, but the Landers uplift is three times the Hector Mine subsidence. In our modeling, we assume a background stress gradient consistent with  $\mu = 0.7$ . Given the assumed crustal stresses, the percentage coseismic reduction in  $E$  required to fit the LOS displacement data is of the order of 1 to 4%, equal to or exceeding the value for the Johnson Valley Fault (about 1%). The percentage softening required to fit the LOS displacements is smaller for higher stress. This suggests that the (fairly high) background deviatoric stress we assume is on the low end of the admissible range.

[51] An alternative modeling approach would have been to require both CZs to be 50% softer than their surroundings and to soften coseismically by 1%, and to fit the LOS displacements by varying the background stress. Doing this, it is difficult to model PMF strain from the Landers and Hector Mine (HM) earthquakes with a single compliant zone. The result is nonsensical background tectonic stresses which are different for the two earthquakes. With this approach it would also be difficult to explain why similarly oriented Mojave compliant zones near the CRF deform coseismically in the opposite sense to the CRF (i.e., consistent with the coseismic stress [Fialko *et al.*, 2002; Fialko, 2004]. Variations in compliant zone stiffness and degree of coseismic softening seem a better explanation than background stress that varies profoundly over very short (kilometer-scale) distances.

## 5.2. Compliant Zone Properties Required by the Finite Element Models

[52] Our Camp Rock Fault models require softening which is generally greater than that observed by Vidale and Li [2003], and a CZ rigidity that exceeds estimates for Mojave compliant zones [e.g., Fialko *et al.*, 2002; Fialko, 2004; Cochran *et al.*, 2009; Peng *et al.*, 2002; Li *et al.*, 1999]. For the Pinto Mountain Fault, the required CZ rigidity is consistent with the seismic and geodetic observations. Our estimate of the extent of coseismic softening of the PMF in response to the Hector Mine earthquake is comparable to that inferred from seismic velocity changes along the Johnson Valley Fault [Vidale and Li, 2003]. For the Landers earthquake, a much greater degree of softening of the Pinto Mountain Fault CZ is required. Greater softening in a larger earthquake, or at a shorter epicentral distance, makes sense regardless of whether the softening is due to dynamic or static stress. This may explain the greater softening of the PMF in the Landers earthquake, but it does not explain our results for CRF, as the CRF and the

JVF are at similar distances to the Hector Mine earthquake rupture. If the central Mojave is experiencing transpression, however, our coseismic softening estimates for the CRF are at the lower bound of the ranges given above (0.5 to 1%) and are consistent with the seismic constraints of Vidale and Li. It is also possible that the coseismically induced damage depends on the time since the last rupture on a given fault zone. This would explain our inference of coseismic softening along the Camp Rock Fault, but no apparent coseismic softening of the Calico fault, which lies closer to the Hector Mine rupture.

[53] For the PMF, a shallow CZ (i.e., model C) is most consistent with our assumption that the CZ is 50% softer than the host rock. The fit of the deepest CZ model to the LOS displacement data looks better qualitatively (Figures 13c and 13d), but a substantially stiffer CZ is required. Given that edges of compliant zones are likely diffuse [Cochran *et al.*, 2009] and that we did not model them that way, the sharp “corners” along the LOS displacement profiles for shallow compliant zones do not justify ruling them out. If we cannot fix the PMF compliant zone  $E$  to 50% of the value for the host rock, we cannot distinguish its depth. If independent evidence of this relative strength became available, however, our results would support a shallow PMF compliant zone (or a compliant zone that narrows at depth, as suggested by trapped wave studies and damage rheology models [e.g., Finzi *et al.*, 2009]).

## 5.3. Absence of Lithostatic Subsidence: Evidence of Incompressible Compliant Zones?

[54] Under lithostatic stress, coseismically softened compliant zones should contract enough under their own weight to cause ground subsidence of several centimeters, not just within the CZ, but in the surrounding region (Figures 13a, 13b, 14a, and 14b). Coalescence of these subsidence “haloes” around individual compliant zones should cause regional coseismic subsidence of several centimeters, which should be geodetically detectable. Such subsidence was not observed in GPS vertical displacement data from the Hector Mine earthquake [Nikolaidis, 2002]. This confirms our conclusion (based on models of individual compliant zones) that contraction of coseismically softened compliant zones in response to gravitational body forces is negligible.

[55] CZs which do not soften coseismically could extend deep into the crust without causing regional subsidence. If we assume that the PMF does not soften coseismically, uplift and subsidence of the compliant zone during the Landers and Hector Mine earthquakes may be explained, though the magnitude of uplift during the Landers earthquake is too low and the (minor) shear across the CZ is not reproduced. Given the possible errors in coseismic stress estimates, this might not seem an insurmountable problem. However, the CRF certainly must soften coseismically: most of its coseismic deformation appears to result from softening and background, deviatoric stress. Although softening is required to explain the shear strain, LOS displacement data across the CRF clearly exclude lithostatic subsidence. Hence, we need to explain how coseismically softened compliant zones can resist contracting under their own weight.

[56] Some ways to limit such subsidence while allowing coseismic softening include assuming that the CZ (1) is very

narrow, (2) has a very high Poisson's ratio, (3) experiences no coseismic change to its bulk modulus, or (4) is elastically anisotropic.

[57] Our models with very narrow compliant zones clearly suppress subsidence (Figures 13a, 13b, and 14b), but these models cannot fit the InSAR LOS displacements due to the narrowness of the uplifting and subsiding zone. A model of a "funnel-shaped" compliant zone, inspired by the results of damage rheology models of fault system generation [Finzi *et al.*, 2009], was developed in the hope that the gravitational subsidence would comprise a smaller proportion of the overall deformation than it does for our tabular models, while producing a broader pattern of strain at the Earth's surface. This did not suppress the subsidence (Figure 14a). Hence option 1 may be ruled out.

[58] The simplest way to overcome the lithostatic subsidence problem, while preserving CZ deformation in response to deviatoric background stress, is to assume that compliant zones are incompressible (option 2). A high  $\nu$  is consistent with seismic studies [e.g., Li and Vidale, 2001]. However, our results would require a  $\nu$  very close to 0.5. More detailed studies are needed to determine the spatial variability of  $\nu$  in compliant zones. It may be sufficient to have a very high  $\nu$  just near the surface, where the gravitational body force is large relative to the shear modulus.

[59] Subsidence may also be suppressed (by option 3) if  $\nu$  increases coseismically as  $E$  decreases, in a way that prevents a coseismic decrease in the bulk modulus ( $K$ ). A constant  $K$  is assumed in some damage rheology models which are used to study the formation and evolution of faults [e.g., Lyakhovskiy *et al.*, 1997; Finzi *et al.*, 2009]. Both  $E$  and  $\nu$  in CZs may either increase or decrease coseismically, depending on changes to microcrack density and pore fluid saturation [Budiansky and O'Connell, 1976]. Furthermore, coseismic dilatancy of shallow fault zone material may have occurred during the 2003 Bam, Iran, earthquake [Fielding *et al.*, 2008]. If  $E$  decreased coseismically in this fault zone,  $\nu$  must have increased.

[60] If dynamic stressing causes most of the coseismic microcracking and softening of compliant zones, the microcrack density should increase coseismically in fault zones throughout the Mojave, presumably as a function of epicentral distance. Assuming similar levels of fluid saturation, elastic properties in all of these compliant zones should be affected in the same sense as they were in the JVF. The trapped wave studies of this fault zone [Vidale and Li, 2003] show similar percentage decreases in both  $V_p$  and  $V_s$ , and this requires an unchanging (or slightly decreasing)  $\nu$ . This is also illustrated by Figure 5: a coseismic increase to  $\nu$  is not possible unless  $R > 1$ , which is not consistent with the JVF  $V_p$  and  $V_s$  data [Vidale and Li, 2003]. Given the similarities of the JVF and the CRF, in terms of proximity to the Hector Mine earthquake rupture and the fact that both faults failed during the 1992 Landers earthquake, the JVF seems a good analogy for the CRF. Thus it seems unlikely that its  $K$  remained constant during the Hector Mine earthquake.

[61] With regard to option 4 above, shear wave velocity anisotropy has been observed within the Hector Mine earthquake rupture zone [e.g., Cochran *et al.*, 2003]. This anisotropy is consistent with roughly N-S oriented, vertical

microcracks in the top few kilometers of the crust. If vertically oriented microcracks are the cause, then the elastic properties of the uppermost crust could be anisotropic as well, with the maximum strength in the vertical direction. It is possible that this could suppress gravitational subsidence relative to other components of coseismic compliant zone deformation.

[62] It is possible that more than one explanation applies. For example, compliant zones might narrow with depth (or soften coseismically only very close to the surface), and have a high Poisson's ratio and anisotropic elastic strength near the surface. Explanations such as this are testable with detailed seismic studies.

## 6. Conclusions

[63] Coseismic strain of Mojave compliant zones includes contributions from both the coseismic stress change and coseismic compliant zone softening, which causes an increment of strain driven by total background stress.

[64] Theoretically, compliant zones which soften coseismically should contract under their own weight, causing both local and regional subsidence during a large earthquake. Since such subsidence is not observed, we conclude that the coseismically softening parts of compliant zones are incompressible and/or that they have anisotropic elastic strength.

[65] Deformation of the Pinto Mountain and Camp Rock Fault compliant zones in response to the Hector Mine and Landers earthquakes includes substantial contributions from the background stress and coseismic softening. These contributions are consistent with a stress state in which static friction coefficient  $\mu$  is of the order of 0.7 or higher.

[66] We find that the coseismically softening parts of compliant zones are of the order of 2 km wide at the Earth's surface, but we cannot constrain how this width varies with depth. If some compliant zones are of the order of 1–2 km wide down to the middle crust (i.e., step overs), and they soften coseismically, they could locally influence coseismic static stress transfer at seismogenic depths.

[67] We do not find a "one size fits all" model of Mojave compliant zones; their properties vary. Given more constraints on their dimensions, elasticity, and coseismic softening, we conclude that crustal stress estimates can be made by modeling compliant zone strain.

[68] Damage models suggest that compliant zones at step overs remain wide to midcrustal depths [Finzi *et al.*, 2009]. If these compliant zones also soften coseismically over their entire depth, models of their coseismic deformation could provide constraints on stresses at seismogenic depths. Hence, compliant zones within step overs are good targets for future study.

[69] **Acknowledgments.** E. Hearn's research on this project was supported by grants from the Southern California Earthquake Center (SCEC) and NSERC. This paper is SCEC contribution 1232. Y. Fialko acknowledges support from NSF (EAR-0450035) and SCEC. Original InSAR data are copyright of the European Space Agency, acquired via the WInSAR Consortium. We would like to thank Andrew Hooper and an anonymous reviewer for their helpful comments on our paper.

## References

Agnew, D. C., S. Owen, Z.-K. Shen, G. Anderson, J. Svarc, H. Johnson, K. E. Austin, and R. Reilinger (2002), Coseismic displacements from

- the Hector Mine, California, earthquake: Results from survey-mode Global Positioning System measurements, *Bull. Seismol. Soc. Am.*, 92(4), 1355–1364.
- Bartley, J. M., A. F. Glazner, and E. R. Schermer (1990), North-south contraction of the Mojave Block and strike-slip tectonics in southern California, *Science*, 248, 1398–1401.
- Brenguier, F., M. Campillo, C. Hadziioannou, N. M. Shapiro, R. M. Nadeau, and E. Larose (2008), Postseismic relaxation along the San Andreas Fault at Parkfield from continuous seismological observations, *Science*, 321, 1478–1481.
- Budiansky, B., and R. O'Connell (1976), Elastic moduli of a cracked solid, *Int. J. Solids Struct.*, 12, 81–97.
- Ciccotti, F., and M. Mulargia (2004), Differences between static and dynamic elastic moduli of a typical seismogenic rock, *Geophys. J. Int.*, 157, 474–477.
- Cochran, E. S., J. E. Vidale, and Y.-G. Li (2003), Near-fault anisotropy following the Hector Mine earthquake, *J. Geophys. Res.*, 108(B9), 2436, doi:10.1029/2002JB002352.
- Cochran, E., Y.-G. Li, P. Shearer, S. Barbot, Y. Fialko, and J. Vidale (2009), Seismic and geodetic evidence for extensive, long-lived fault damage zones, *Geology*, doi:10.1130/G25306A.1, in press.
- Dokka, R. K., and K. Y. Macaluso (2001), Topographic effects of the Eastern California Shear Zone in the Mojave Desert, *J. Geophys. Res.*, 106, 30,625–30,644.
- Dokka, R. K., T. M. Ross, and G. Lu (1998), The Trans Mojave-Sierran shear zone and its role in early Miocene collapse of southwestern North America, in *Continental Transpressional and Transtensional Tectonics*, edited by R. E. Holdsworth, R. A. Strachan, and J. F. Dewey, *Geol. Soc. Spec. Publ.*, vol. 135, pp. 183–202.
- Eissa, E. A., and A. Kazi (1988), Relation between static and dynamic Young's Moduli of Rocks, *Int. J. Rock Mech. Min Sci Geomech. Abstr.*, 25(6), 479–482.
- Faulkner, D. R., T. M. Mitchell, D. M. Healy, and M. J. Heap (2006), Slip on "weak" faults by the rotation of the regional stress in the fracture damage zone, *Nature*, 444, 922–925.
- Fialko, Y. (2004), Probing the mechanical properties of seismically active crust with space geodesy: Study of the co-seismic deformation due to the 1992  $M_w$ 7.3 Landers (southern California) earthquake, *J. Geophys. Res.*, 109, B03307, doi:10.1029/2003JB002756.
- Fialko, Y., D. Sandwell, D. Agnew, M. Simons, P. Shearer, and B. Minster (2002), Deformation on nearby faults induced by the 1999 Hector Mine earthquake, *Science*, 297, 1858–1862.
- Fielding, E. J., P. R. Lundgren, R. Burgmann, and G. J. Funning (2008), Shallow fault-zone dilatancy recovery after the 2003 Bam earthquake in Iran, *Nature*, in press.
- Finzi, Y., V. Lyakhovskiy, E. Hearn, and Y. Ben Zion (2009), Structural properties and deformation patterns of evolving strike-slip faults: Numerical simulations incorporating damage rheology, *Pure Appl. Geophys.*, in press.
- Gratier, J.-P., P. Favreau, and F. Renard (2003), Modeling fluid transfer along California faults when integrating pressure solution crack sealing and compaction processes, *J. Geophys. Res.*, 108(B2), 2104, doi:10.1029/2001JB000380.
- Hamiel, Y., and Y. Fialko (2007), Structure and mechanical properties of faults in the North Anatolian Fault system from InSAR observations of coseismic deformation due to the 1999 Izmit (Turkey) earthquake, *J. Geophys. Res.*, 112, B07412, doi:10.1029/2006JB004777.
- Hearn, E., and R. Bürgmann (2005), The effect of elastic layering on inversions of GPS data for coseismic slip and resulting stress changes: Strike-slip earthquakes, *Bull. Seismol. Soc. Am.*, 95, 1637–1653.
- Ide, J. M. (1936), Comparison of statically and dynamically determined Young's modulus of rocks, *Proc. Natl. Acad. Sci., U. S. A.*, 22, 81–92.
- Jones, L., and D. Helmberger (1998), Earthquake source parameters and fault kinematics in the Eastern California Shear Zone, *Bull. Seis. Soc. Am.*, 88, 1337–1352.
- Kaverina, A., D. Dreger, and E. Price (2002), The combined inversion of seismic and geodetic data for the source process of the 16 October 1999 Mw 7.1 Hector Mine, California, earthquake, *Bull. Seismol. Soc. Am.*, 92, 1266–1280.
- Lewis, M. A., Z. Peng, Y. Ben Zion, and F. L. Vernon (2005), Shallow seismic trapping structure in the San Jacinto Fault zone near Anza, California, *Geophys. J. Int.*, 162, 867–881.
- Li, Y.-G., and J. Vidale (2001), Healing of the shallow fault zone from 1994–1998 after the 1992 M7.5 Landers, California earthquake, *Geophys. Res. Lett.*, 28, 2999–3002.
- Li, Y.-G., P. C. Leary, K. Aki, and P. Malin (1990), Seismic trapped modes in the Oroville and San Andreas fault zones, *Science*, 249, 763–766.
- Li, Y.-G., K. Aki, J. Vidale, and F. Xu (1999), Shallow structure of the Landers Fault Zone from explosion-generated trapped waves, *J. Geophys. Res.*, 104, 20,257–20,275.
- Li, Y.-G., J. E. Vidale, S. M. Day, D. D. Oglesby, and E. Cochran (2003), Postseismic fault healing on the rupture zone of the 1999 M 7.1 Hector Mine, California, earthquake, *Bull. Seismol. Soc. Am.*, 93, 854–869.
- Li, Y.-G., P. Chen, E. Cochran, J. Vidale, and T. Burdette (2006), Seismic evidence for rock damage and healing on the San Andreas Fault associated with the 2004 M 6.0 Parkfield earthquake, *Bull. Seis. Soc. Am.*, 96, S349–S363, doi:10.1785/0120050803.
- Lyakhovskiy, V., Y. Ben-Zion, and A. Agnon (1997), Distributed damage, faulting, and friction, *J. Geophys. Res.*, 102, 27,635–27,649.
- Malvern, L. E. (1969), *Introduction to the Mechanics of a Continuous Medium*, Prentice-Hall, Englewood Cliffs, N. J.
- Nikolaïdis, R. M. (2002), Observations of geodetic and seismic deformation with the Global Positioning System, Ph.D. dissertation, Univ. of Calif., San Diego, La Jolla.
- Peng, Z., and Y. Ben Zion (2006), Temporal changes of shallow seismic velocity around the Karadere-Düzce Branch of the North Anatolian Fault and strong ground motion, *Pure Appl. Geophys.*, 163, 567–600.
- Peng, Z., Y. Ben Zion, Y. Zhu, and A. Michael (2003), Inference of a shallow fault zone layer in the rupture zone of the 1992 Landers, California earthquake from locations of events generating trapped waves and travel time analysis, *Geophys. J. Int.*, 155, 1021–1041.
- Saucier, F., and E. Humphreys (1993), Horizontal crustal deformation in Southern California from joint models of geologic and very long baseline interferometry measurements, in *Crustal Dynamics: Contributions of Space Geodesy to Geodynamics*, *Geodyn. Ser.*, vol. 23, edited by D. E. Smith and D. L. Turcotte, pp. 139–176, AGU, Washington, D. C.
- Sibson, R. H. (1974), Frictional constraints on thrust, wrench and normal faults, *Nature*, 249, 542–544.
- Simons, M., Y. Fialko, and L. River (2002), Coseismic deformation from the 1999  $M_w$ 7.1 Hector Mine, California, earthquake as inferred from InSAR and GPS Observations, *Bull. Seismol. Soc. Am.*, 92, 1390–1402.
- Spudich, P., and K. Olsen (2001), Fault zone amplified waves as a possible seismic hazard along the Calaveras Fault in central California, *Geophys. Res. Lett.*, 28, 2533–2536.
- Suppe, J. (1985), *Principles of Structural Geology*, Prentice-Hall, Englewood Cliffs, N. J.
- Townend, J., and M. D. Zoback (2004), Regional tectonic stress near the San Andreas fault in central and southern California, *Geophys. Res. Lett.*, 31, L15S11, doi:10.1029/2003GL018918.
- Vidale, J., and Y.-G. Li (2003), Damage to the shallow Landers fault from the nearby Hector Mine earthquake, *Nature*, 421, 524–526.

Y. Fialko, Scripps Institution of Oceanography, University of California, San Diego, 9500 Gilman Drive, La Jolla, CA 92093, USA. (yfialko@ucsd.edu)

E. H. Hearn, Department of Earth and Ocean Sciences, University of British Columbia, 6339 Stores Road, Vancouver, BC V6T 1Z4, Canada. (ehearn@eos.ubc.ca)